



Hydrogen Fuel System for Gas Turbines

Nicholas Njopa-Kaba, Maddie Hall,
Christian Garry, Samuel Berry, Vanessa
Ohanebo, Henry Wong

MARCH 2022

Project ID:
L2AHTB2

Project Supervisors:
Alton Horsfall
Tom Bray

Executive Summary

Currently, aviation accounts for 2-3 % of CO₂ global emissions. Without decarbonisation, it is predicted that aviation will be responsible for 22 % of global CO₂ emissions by 2050 [1]. Increased government spending and private investment towards the development of widespread hydrogen infrastructure will help smooth the transition as hydrogen becomes economically viable as an alternative fuel source. This report outlines the first step at decarbonising the aviation industry with a detailed design concept of a liquid hydrogen fuel system for a narrow-body regional jet.

Contents

Executive Summary	1
Nomenclature	2
1 Introduction	4
2 Project Scope and User Requirements	5
3 Fuel System	6
3.1 Overall Fuel System Architecture	6
3.2 Weight Requirements	7
3.3 Range Estimation: E190 using Liquid Hydrogen Fuel	7
3.4 Tanks	8
3.4.1 Tank Placement	8
3.4.2 Tank Sizing and Dimensions	9
3.4.3 Tank Materials	10
3.4.4 Tank Insulation Methods	13
3.4.5 LH ₂ Crossfeed System	17
3.4.6 Tank Venting System	18
3.4.7 Pressure Generation System	20
3.4.8 Tank Level Sensing	20
3.4.9 Tank Temperature and Pressure	21
3.4.10 Fuelling and Defuelling	21
3.4.11 Tank Cut-outs: Stress Analysis	22
3.4.12 Boil-Off within Tanks	24
3.5 Engine Fuel Delivery	25
3.5.1 Line Sizing	25
3.5.2 Pipe Insulation	27
3.5.3 Heat Exchanger	29
3.5.4 Leak Detection	35
3.5.5 Boost Pump	37
3.6 APU Fuel Delivery	38
4 Sustainability	38
4.1 NO _x emissions	39
4.2 Weight Minimisation	39
4.3 Carbon Footprint	39
5 Safety	40
6 Commercial Considerations	41
7 Code of Practice	42
8 Discussion	43
9 Further Work	43

10 Conclusion	44
11 Project Schedule	44
References	46
Contributions	48

Nomenclature

ΔP_{loss}	Pressure loss, Pa	C	Heat Capacity rate, J/Ks
\dot{m}_{air}	Mass flow rate of air, kg/s	c	'c' factor
\dot{m}_{H_2}	Mass flow rate of hydrogen, kg/s	C_D	Coefficient of drag
\dot{Q}	Volumetric flow rate, W	C_L	Coefficient of lift
\dot{W}_{pump}	Maximum pump power requirement, W	c_p	Specific heat capacity, J/kgK
ϵ	Effectiveness	C_r	Heat capacity ratio, m
ϵ_m	Emissivity	d	Pipe Diameter, m
η_{pump}	Pump Efficiency	D_i	Inner pipe diameter m
λ	Thermal Conductivity, W/mK	D_o	Outer pipe diameter, m
λ_f	Foam thermal Conductivity, W/mK	E	Function of effectiveness
μ	Dynamic viscosity, Ns/m^2	f	Friction factor
ρ	Density, kg/m^3	FOS	Factor of Safety
σ_∞	Far field uniaxial stress, W/m^2K^4	g	Acceleration due to gravity, $9.81 m/s^2$
$\sigma_{\theta\theta}$	Tangential stress	$GH2$	Gaseous Hydrogen
σ_{mws}	Maximum working stress, MPa	h	Convection heat transfer coefficient, W/m^2K
σ_{SB}	Stefan Boltzmann Constant, W/m^2K^4	h_{losses}	head losses, m
θ	Angle, $^\circ$	h_{pump}	Pump head loss, m
A	Surface area, m^2	I	Current, A
a	Minor ellipse radius, m	K	K Factor
A_{cs}	Cross sectional area, m^2	k	Thermal conductivity, W/mK
b	Major ellipse radius, m	L_{prism}	Length of tank without bulkheads, m
		L_{wire}	Wire length, m
		$LH2$	Liquid Hydrogen

m	mass, kg	$T_{c,o}$	Cold fluid outlet temperature, K
NTU	Number of transfer units	$T_{h,i}$	Hot fluid inlet temperature, K
Nu	Nusselt number	$T_{h,o}$	Hot fluid outlet temperature, K
P	Pressure, MPa	T_{surr}	Cold boundary temperature, K
P_h	Hydrostatic force, N	T_{VCS}	Temperature of vapour cooled shield, K
$P_{internal}$	Internal pressure, MPa	$TSFC$	Thrust Specific Fuel Consumption, g/kNs
P_{IV}	Power, W	U	Overall heat transfer coefficient, W/mK
Pr	Prandtl number, W/m^2K^4	u	Pipe flow velocity, m/s
Q	Heat Flow, W	V	Volume, m^3
R	Resistance, Ω	v	Flow speed, m/s
R	Universal gas constant, 8.314 J/molK	V_e	Maximum erosional velocity, m
$R(\Phi)$	Effective radius, m	V_{bulk}	Single bulkhead volume, m^3
R_{cond}	Solid Conduction Contribution, K/W	V_{plane}	Plane Speed, m/s
R_{rad}	Radiation Contribution, K/W	V_{prism}	Volume of tank without bulkheads, m^3
Re	Reynolds number	V_{tank}	Total tank volume, m^3
SFC	Specific fuel consumption, $g/kN \cdot s$	V_{volts}	Voltage, V
T_C	Temperature at cold boundary, K	VCS	Vapour Cooled Shield
T_f	Average foam temperature, K	W_0	Initial Mass of Plane, kg
T_H	Temperature at hot boundary, K	W_1	Final Mass of Plane, kg
T_s	Hot boundary temperature, K	x	Thickness, mm
$T_{c,i}$	Cold fluid inlet temperature, K		

1 Introduction

Air travel is notorious for its high carbon footprint. In 2019 the aviation industry produced 915 million tonnes of CO₂ [2]. As progress is made towards a more sustainable future, it is essential that air travel is decarbonised. This need is greater than ever before particularly in the wake of COP26 now that almost 200 countries have pledged to reduce their CO₂ emissions with the aim of limiting global temperature rise to 1.5°C. Hydrogen is receiving enormous global attention as an exciting alternative fuel source that promises to reduce or even eliminate carbon emissions in a vast range of industries. The UK, with a legally binding commitment to achieve net zero by 2050, has set out an extensive hydrogen strategy with the ambition of reaching a low carbon hydrogen production capacity of 5 GW by 2030 [3]. The attention hydrogen is receiving is not unwarranted. Hydrogen is the most abundant element in the universe, the combustion of hydrogen does not produce any CO₂ and with a lower heating value (LHV) of approximately 120 MJ/kg, hydrogen has the highest gravimetric density of any known substance [4]. This makes it an ideal fuel source. Liquid hydrogen (LH₂) has been used as rocket fuel for decades [5], however there are ambitious plans worldwide to utilise hydrogen in a much greater variety of applications.

In this report, the design of a hydrogen fuel system for gas turbines is presented. A major aim of this project is to design a system compatible with existing aircraft. The Embraer 190 was selected as an appropriate narrow-body regional jet to serve as a reference aircraft throughout the project. In order to store enough hydrogen to meet the energy requirements of a conventional aircraft, the fuel tanks store LH₂, that is gasified before delivery to the engines or APU (Auxiliary Power Unit) of the aircraft. With a boiling temperature of 20 K at atmospheric pressure, the storage and transportation of LH₂ within the system presents a significant design challenge. The overall fuel system design is detailed within the report including the design of the tanks, insulation methods, venting system, heat exchanger and other key aspects of the hydrogen fuel system. The wider challenges and context of the project such as sustainability, commercial considerations, safety and design limitations are discussed throughout.

Project Scope and User Requirements

Aim:
To design a liquid hydrogen fuel system to support the power requirements for the Embraer 190 (narrow body, regional jet).

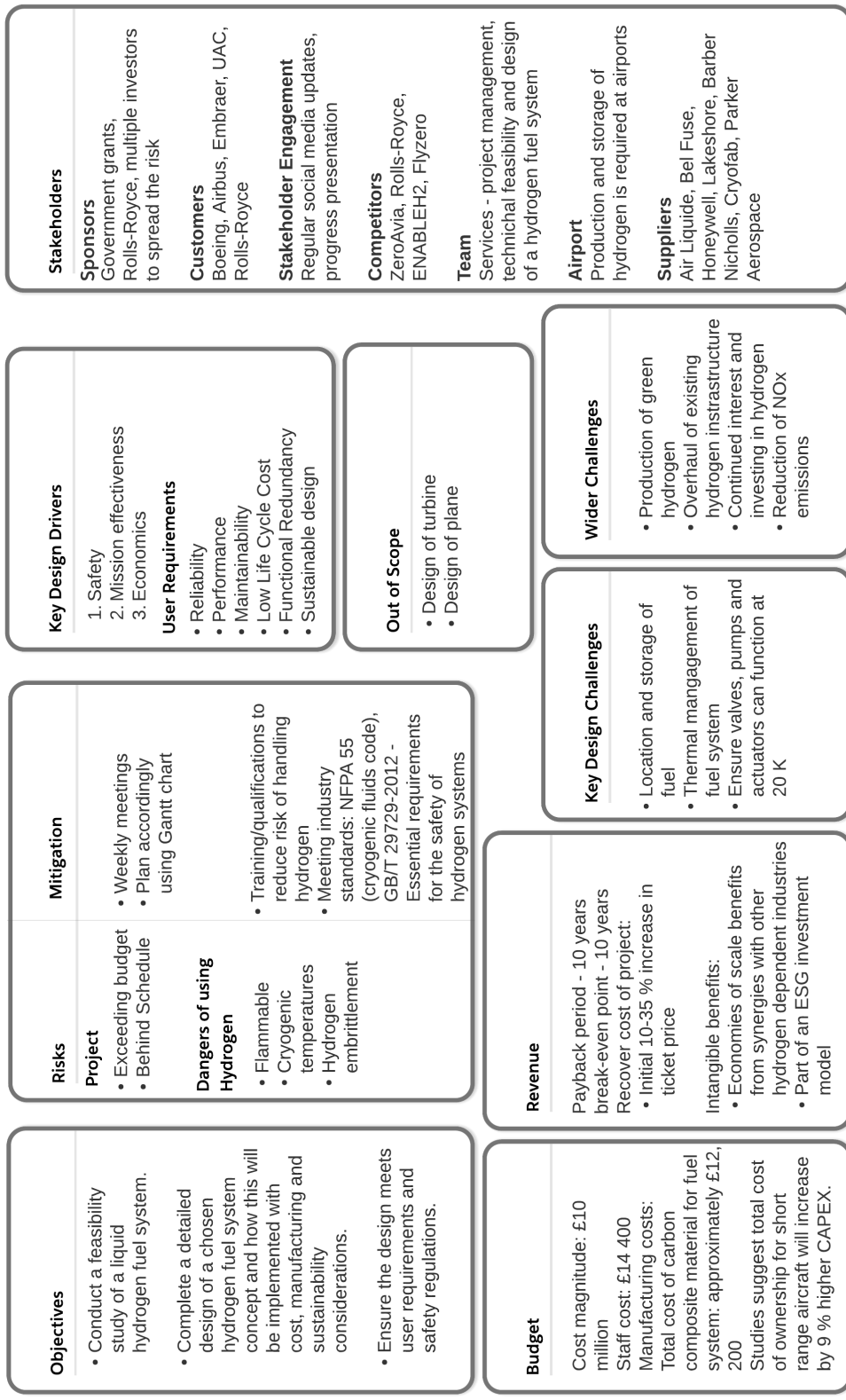


Figure 1: Project Scope Canvas [6]

3 Fuel System

3.1 Overall Fuel System Architecture

Described in depth in this chapter, the overall fuel system is depicted in Figure 2. This schematic diagram illustrates the various ways in which hydrogen can flow through the fuel system. An underside view of a CAD model of the fuel system can be found in Figure 3

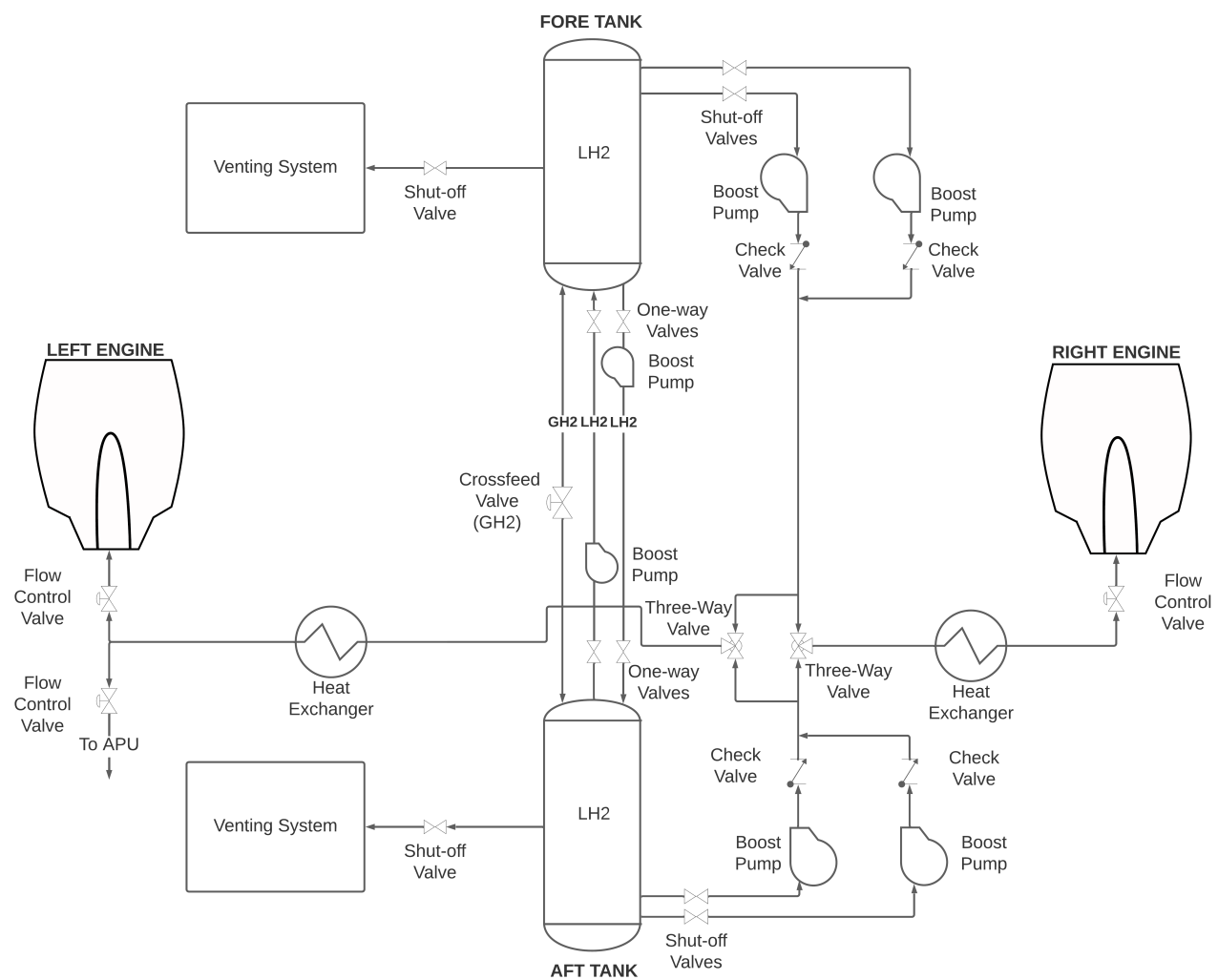


Figure 2: Fuel System Schematic

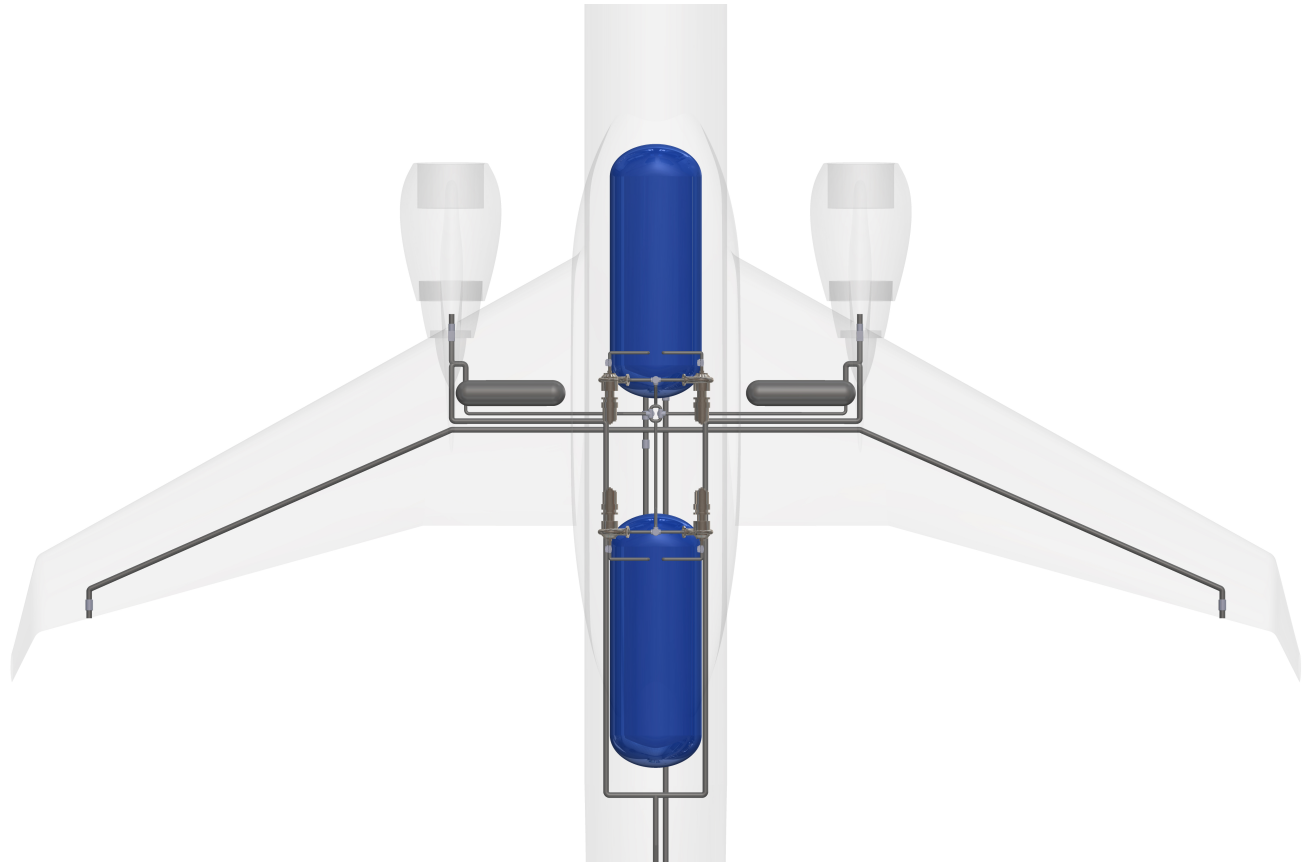


Figure 3: Overall Fuel System (Underside view)

3.2 Weight Requirements

In order to determine the weight requirements, the maximum landing mass was used because fuel jettisoning was determined to add little benefit. Although the energy equivalent ratio of hydrogen to kerosene is 1:2.8 kg respectively, incorporating structural weight added to support 1kg of fuel [7], the weight ratio changes to a minimum of 2:3.1 kg even when using advanced composite technologies highlighted in section 3.2.2. This means that the proportion of fuel available to be jettisoned decreases by 40% for the same energy requirements. Table 1 shows the comparison of the original weights of the Embraer 190 and the target mass requirements of the aircraft with the new fuel system design.

Table 1: Target and orginal mass requirements of Embraer 190 aircraft

	Kerosene (Original) / kg	Hydrogen (Target) / kg
Maximum Take-Off Mass	50,300	43,000
Maximum Landing Mass	43,000	43,000
Maximum Payload Mass	13,063	13,063
Basic Operating Mass	27,750	27,750

3.3 Range Estimation: E190 using Liquid Hydrogen Fuel

The ICAO (International Civil aviation organisation) states that planes must have enough reserve fuel, in case of an emergency, for an additional 30 minutes of flight for jet engine aircraft, and 45 minutes of flight for reciprocating engine aircraft [8]. The E190 uses two GE CF34-10E turbofan engines with a thrust specific fuel consumption (TSFC) of 18 g/kNs using kerosene. The specific energy of hydrogen (120 MJ/kg) is 2.8 times larger than the specific energy of kerosene (42.8 MJ/kg). This conversion factor is used to predict the TSFC for the two GE

turbofan engines using hydrogen fuel to be 2.8 times smaller than when using kerosene. Therefore, the TSFC for the GE turbofan engines using hydrogen is 6.42 g/kNs.

The final mass of the plane, W_1 , accounts for the empty mass of the plane (27,750 kg) and the payload (13,063 kg). The initial mass, W_0 , accounts for W_1 and the mass of the fuel. The additional reserve fuel required can be calculated using Breguet's endurance equation. The ratio of coefficient of lift to coefficient of drag (C_L/C_D) is represented as the ratio of the mass of the plane (43,000 kg) to the thrust (2 x 90.6 kN GE CF34-10E engines). Therefore, 45 minutes of additional flight requires 314 kg of hydrogen.

$$Endurance = \frac{1}{TSFC} \times \frac{C_L}{C_D} \times \ln \frac{W_0}{W_1} \quad (1)$$

The Breguet range equation is then used to calculate the mass of fuel required to give the E190 a maximum range of 2000 km. This is a typical range for a regional aircraft, ensuring the E190 would be able to serve routes as long as London to St Petersburg. However, it is anticipated that hydrogen powered jets will be used on much shorter routes, such as London to Berlin (930 km). The 314 kg of hydrogen reserve fuel will now be included in W_0 and W_1 when using the Breguet range equation. The speed (V_{plane}) of the plane can be assumed to be constant at cruising speed (230 m/s) throughout the flight as the ascent and descent periods are minimal compared to the overall flight time for a regional jet. By the same argument, the air density can be assumed to remain constant at cruising altitude throughout the flight. The amount of fuel required for a range of 2000 km is 1100 kg. Therefore, the total hydrogen fuel, including reserve fuel, that will be stored on the plane is 1414 kg.

$$Range = \frac{V_{plane}}{TSFC} \times \frac{C_L}{C_D} \times \ln \frac{W_0}{W_1} \quad (2)$$

3.4 Tanks

The fuel tanks of a liquid hydrogen powered plane are a crucial element of the overall system design. The placement of the tanks was carefully considered to determine an optimal solution given the design of existing narrow-body regional aircraft.

3.4.1 Tank Placement

Several tank arrangements were considered, as shown in Figure 4. Designs were compared using several criteria such as disruption to plane layout, the proximity of the tanks to the engines, and any affects of the centre of gravity of the plane.

There are additional challenges when selecting tank parameters for a LH2 tank when compared to conventional tanks used for other fuels. For example, the tank storage must minimise boil off rates in the tank by having a small surface area to volume ratio, whilst best fitting the available space in the plane. For LH2 storage on the ground, singular spherical tanks are used due to their small surface area to volume ratio, minimising boil off rates and the tank mass. However, a spherical tank would not be suitable fitting into the long fuselage body and instead a prism tank would best occupy the available space. Initially a singular prism tank was chosen under the cabin floor. However, it was found that the landing gears of plane disrupted a singular tank located centrally. Therefore, a split tank design as shown in Figure 5 consisting of a fore and aft tank under the cabin floor was chosen to create redundancy if faults arise and for better fuel positioning control via a cross-feed system between the two tanks.

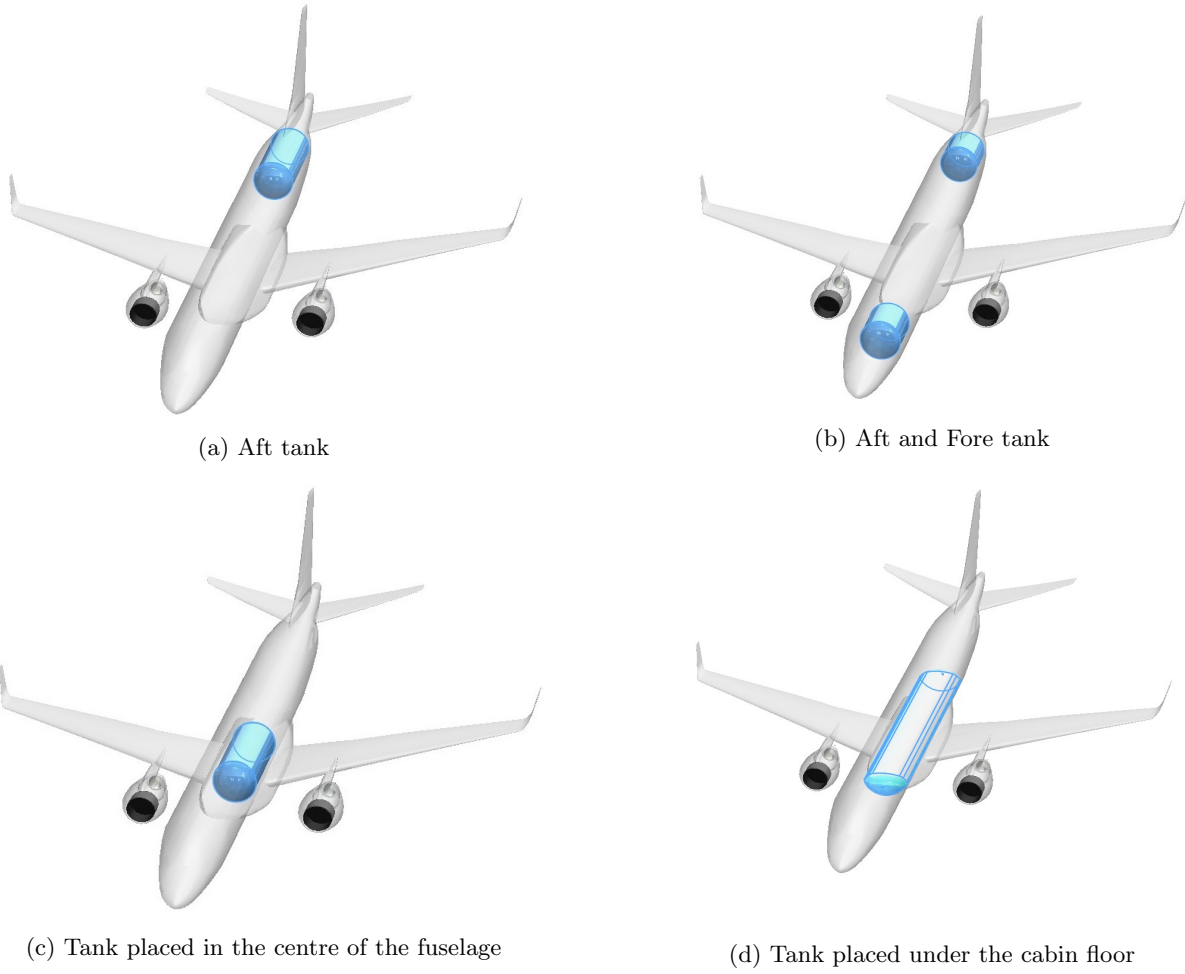


Figure 4: Tank Placement Concepts

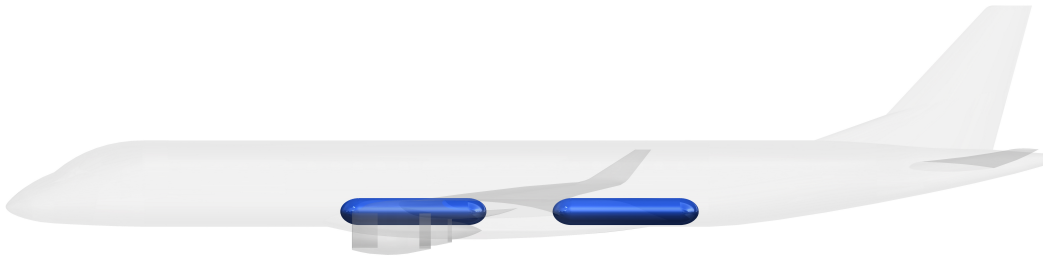


Figure 5: Chosen design - Fore and aft tanks under the cabin floor

3.4.2 Tank Sizing and Dimensions

An elliptical tank shape was chosen as it best fills the fuselage under-cabin cross sectional area, minimising the length and so the weight of the tank. The 1414 kg of liquid hydrogen occupies 19.92 m³ of volume, and according to [9] 3% extra volume should be available to accommodate boil off before flight. Therefore, the total tank volume required is 20.53 m³.

The elliptical tanks have two hemi-ellipsoidal bulkheads on either end of the tanks. NASA recommend for the bulkhead ellipsoids a ratio $a/c = 1.66$ offers the best combination of tank weight and tank length, where a is the

minor ellipse radius as shown in Figure 6 and c is the 3rd ellipsoid dimension [10]. This ratio gives the length of each bulkhead (c) as 0.349 m. Equations (3 - 5) are used to calculate the length of the elliptical prism segment of the tank (L_{prism}) and then the total length of each tank is calculated by accounting for the additional length of the two bulkheads on either end of the tank. The total length of each tank is 5.13 m.

$$V_{prism} = V_{tank} - 2V_{bulk} \quad (3)$$

$$L_{prism} = \frac{V_{prism}}{A} \quad (4)$$

$$L_{tank} = L_{prism} + 2L_{bulk} \quad (5)$$

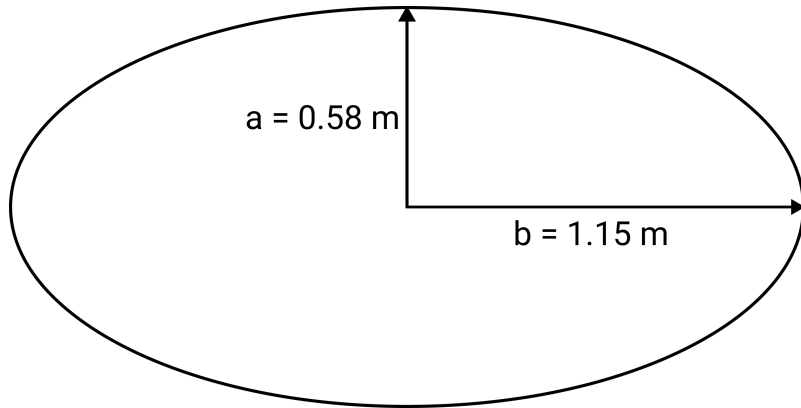


Figure 6: Tank Cross section major and minor axis

3.4.3 Tank Materials

After determining the tank dimensions and internal tank pressure, the next stage in development was designing a tank that meets the mass and insulation requirements, whilst reducing the heat flux into the tank and therefore minimising boil-off.

A lightweight and reusable liquid hydrogen storage tank solution that can operate under cryogenic conditions has been developed with a focus on using innovative, high performance materials in order to optimise the mass to volume ratio. Figure 7 shows different construction options for pressure vessels as classified by the American Society of Mechanical Engineers; with the final tank design following type III. The design of the tank is divided into two main components: the inner tank vessel made from a carbon fibre composite structure and the outer vessel made of stainless steel, maintaining a vacuum which retains the insulating materials in an effort to minimise the heat leak into the liquid hydrogen (LH₂). This section takes an overview into the design challenges during the development of the tank concept and the selection process for the chosen tank materials and manufacturing considerations.

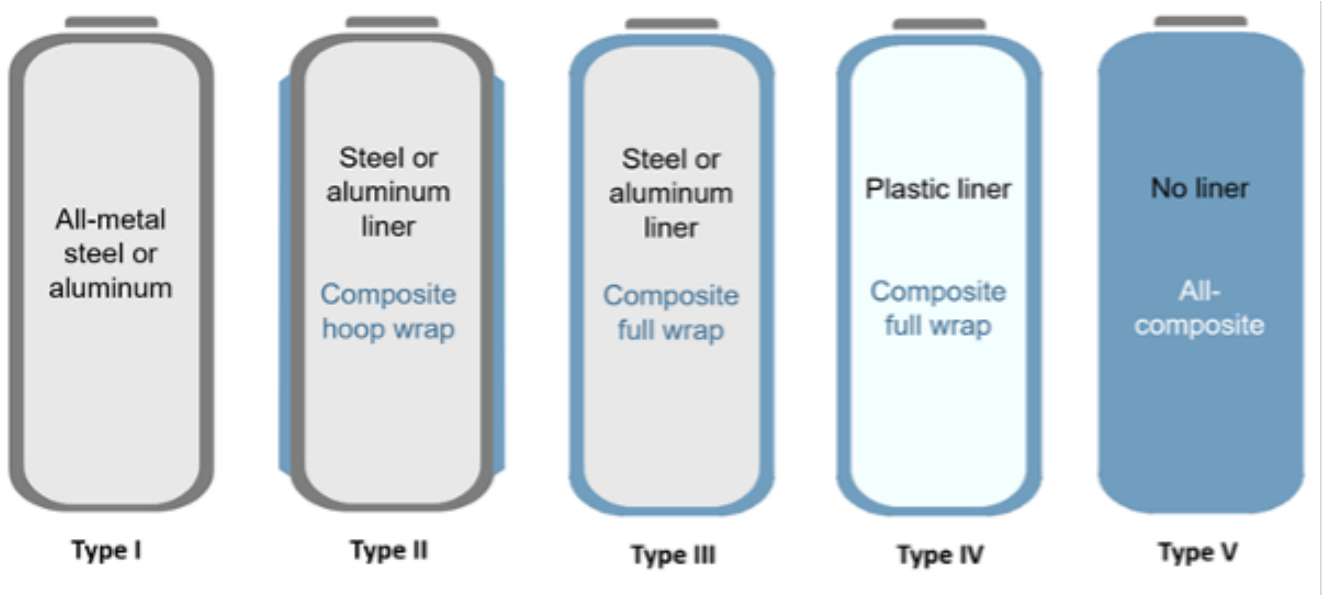


Figure 7: Construction of pressure vessels as per the American Society of Mechanical Engineers [11]

Inner Tank: Carbon Fibre Composite

The use of carbon fibre reinforced polymers is becoming more prevalent in the aerospace and aviation industry, with projects such as NASA's X57 Maxwell aircraft [12] incorporating carbon fibre into the wing design due to the enhanced structural properties provided. In regard to their use in cryogenics, this is still a developing technology, taking for example the Lockheed Martin X33 project [13], consisting of two carbon tanks, which failed during testing due to the debonding of the carbon fibre layers, as a result of gaseous hydrogen (GH₂) infiltrating into the core. It is evident that carbon fibres offer optimal weight properties, but further research and testing is needed before they can be incorporated comfortably for future cryogenic use.

Structural efficiency is one of the considerations at the forefront of the tank design as it is an important aspect to finding lighter solutions when designing load bearing components for aircrafts. As a result, the materials used in the inner tank vessels diverge from commonly used cryogenic metals such as aluminium or steel alloys and instead incorporate carbon fibre reinforced polymers, which offer a much higher specific stiffness and strength and can therefore provide significant weight reduction. The comparison between carbon fibre and other materials considered in the design process as shown in Table 2 highlights the advantages of selecting carbon as the inner tank material. Material analysis shows that using carbon fibre in comparison to aluminium reduces the weight of the inner tank vessel by approximately 42%, proving carbon to be the better choice in terms of weight optimisation. As highlighted in Figure 1 the use of a metal liner is essential in the tank design due to the fact that carbon composite is porous to hydrogen and so the incorporation of a high thermal conductivity aluminium liner to the inner tank vessel provides a permeation and outgassing barrier, effectively protecting the vacuum space.

Table 2: Tank Material Properties

Material	Density (kg/m ³)	Yield Strength (MPa)	Specific Stiffness (MNm/kg)
Aluminium 5083	2650	228	27.2
Aluminium 2219	2840	290	26.0
Stainless Steel 304	8000	215	23.8
Carbon IM7/997	1600	1050	187.5

Structural Optimisation: Honeycomb Sandwich Structure

Sandwich construction has been implemented into the tank design, where two carbon fibre face-sheets are bonded to a lightweight honeycomb core using an adhesive. This is a common technique used in aerospace due to the high specific mechanical properties provided as well as additional design versatility. As a result, the inner tank vessel is

split into three sections: the inner and outer face-sheets and the honeycomb core as shown in the diagram in Figure 8. The tensile and compressive loads are carried by the carbon sheets whilst the honeycomb core absorbs the shear components of force and stiffness by distancing the carbon face-sheets from the neutral axis. And so, increasing the thickness of the corrugated core increases the relative bending strength and stiffness of the structure for only a fractional increase in weight as shown in the table in Figure 9. A configuration thickness of 1.07 mm for each carbon face-sheet and 2.14mm for core was selected resulting in a 3.5 fold increase in bending strength for just a 3% weight increase.

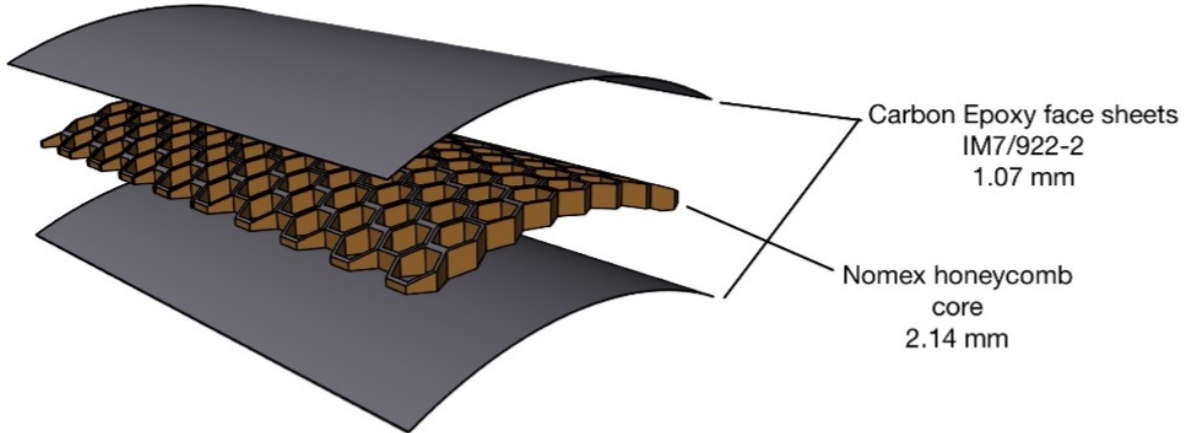


Figure 8: Dimensions of honeycomb sandwich structure

Relative Bending Stiffness	1	7.0	37
Relative Bending Strength	1	3.5	9.2
Relative Weight	1	1.03	1.06

Figure 9: Structural efficiency of sandwich panels [14]

Manufacturing Methods

The carbon layers of the inner tank vessel are constructed from a continuous IM7 unidirectional carbon fibre through wet filament winding which yields variability in the tank shape and so is commonly used in creating complex shaped vessels. The use of one continuous fibre provides very good material stiffness and strength. Initially, the carbon fibre is run through an epoxy resin bath which stabilises the fibre before it is fixed in a specific geometric arrangement. The resin wetted carbon fibre is then wound at 45° angles around a rotating mandrel, creating the inner and outer face sheets in the desired geometry.

The core in-between the face sheets consists of a phenolic Nomex honeycomb made with aramid paper. Lines of glue are applied to numerous flat sheets of aramid paper, before the sheets are stacked. Rods are used to create openings in the paper, creating a honeycomb structure. This is then put in a stabilization oven to retain the hexagonal shape before being dipped and cured in a phenolic resin. The structure is then cut into sheets of the desired thickness, forming the Nomex honeycomb sheets ready to be bonded with an adhesive to the inner and outer carbon shells.

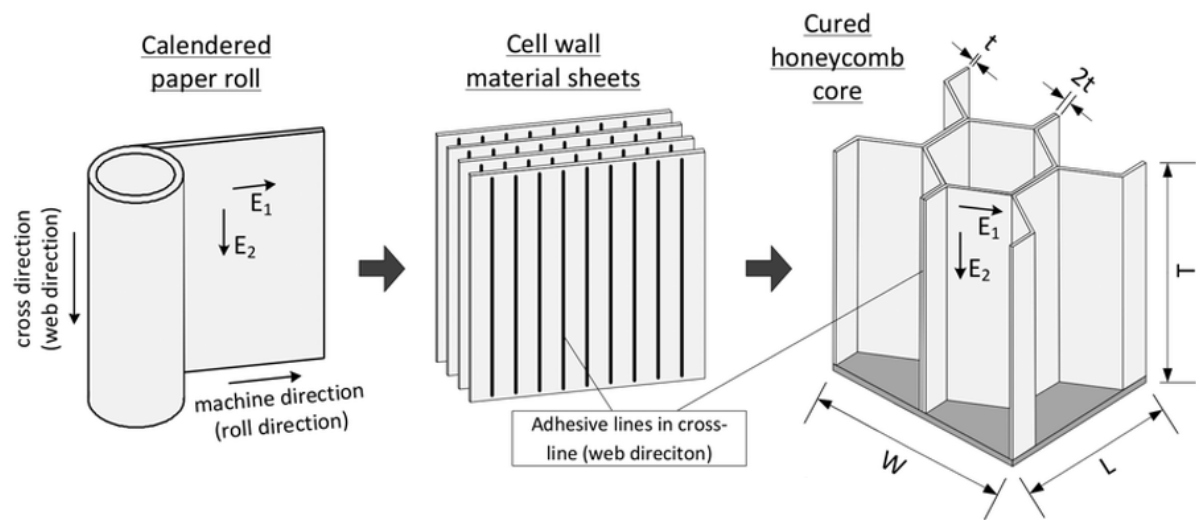


Figure 10: Manufacturing process of Nomex honeycomb [15]

3.4.4 Tank Insulation Methods

The addition of insulation is essential for the tank as its absence can result in a boil-off rate that would render the use of liquid hydrogen impractical. The tank insulation comprises of a vacuum jacketed system consisting of Multi-Layer Insulation (MLI), a spray on foam and a vapour cooled shield. In order to estimate the insulation requirements, a heat flow analysis was conducted, evaluating each section in turn to calculate an overall heat flow into the tank for use in boil off calculations. This section covers how the insulation methods used as shown in Figure 11 impact the heat flow into the system.

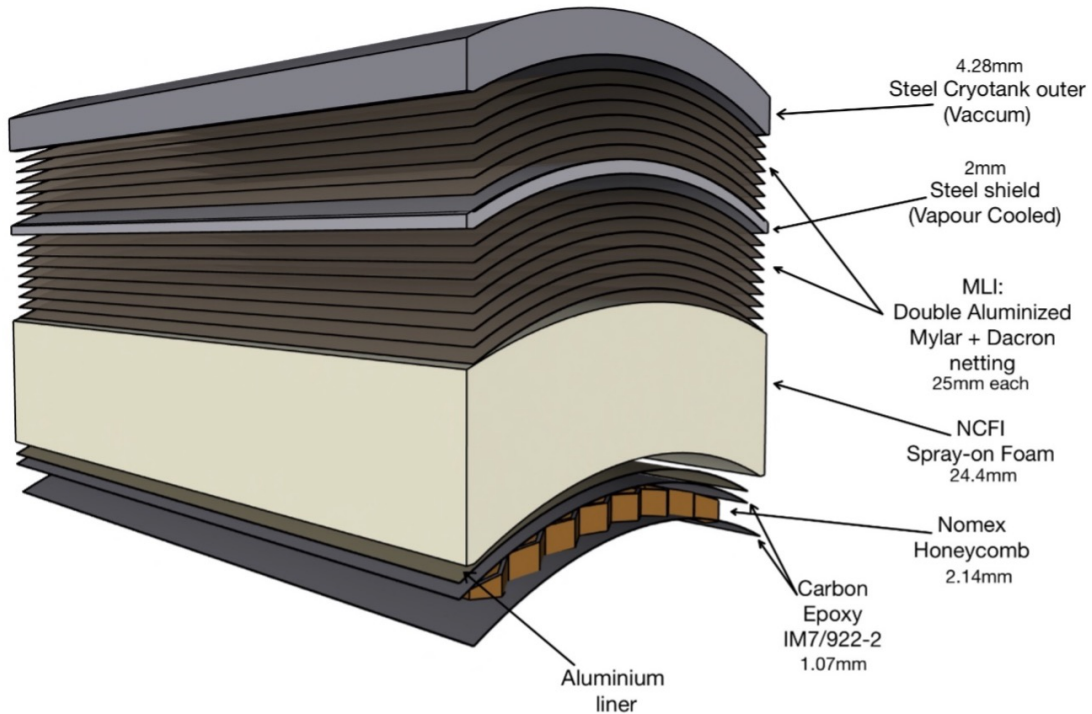


Figure 11: Exploded View of Tank Insulation

Initially, the heat flux calculations involved the use of the Lockheed equation as presented in Lockheed's study for NASA [16]; but one of the main challenges was the derivation of the insulation's temperature gradient in addition to calculating the empirical constants necessary. As a result, a thermal modelling approach was implemented instead where the thermal resistance of each insulation section is calculated; this uses the hot and cold temperature boundaries removing the need to derive a temperature gradient. The tank has been modelled as a one dimensional, steady state model as shown in 12. Heat transfer by radiation and conduction has been analysed, whilst the effect of convection is considered negligible due to the vacuum space eliminating air flow. Using the model and assumptions made, the heat flow (Q_{hf}) is calculated as

$$Q_{hf} = \frac{T_H - T_{VCS}}{R_{cond,1} + \left(\frac{1}{R_{cond,2}} + \frac{1}{R_{rad,2}} \right)^{-1}} + \frac{T_{VCS} - T_C}{\left(\frac{1}{R_{cond,3}} + \frac{1}{R_{rad,3}} \right)^{-1} + R_{cond,4} + R_{cond,5}} \quad (6)$$

where R_{rad} and R_{cond} are the radiation and solid conduction contributions to thermal resistance whilst T_H and T_C are the temperatures at the hot and cold boundaries respectively; with T_{VCS} being the temperature of the vapour cooled shield. Using this modelling approach, the final heat flow came to 396 W. The following chapters outline the heat transfer calculations and considerations for each specific section of the tank.

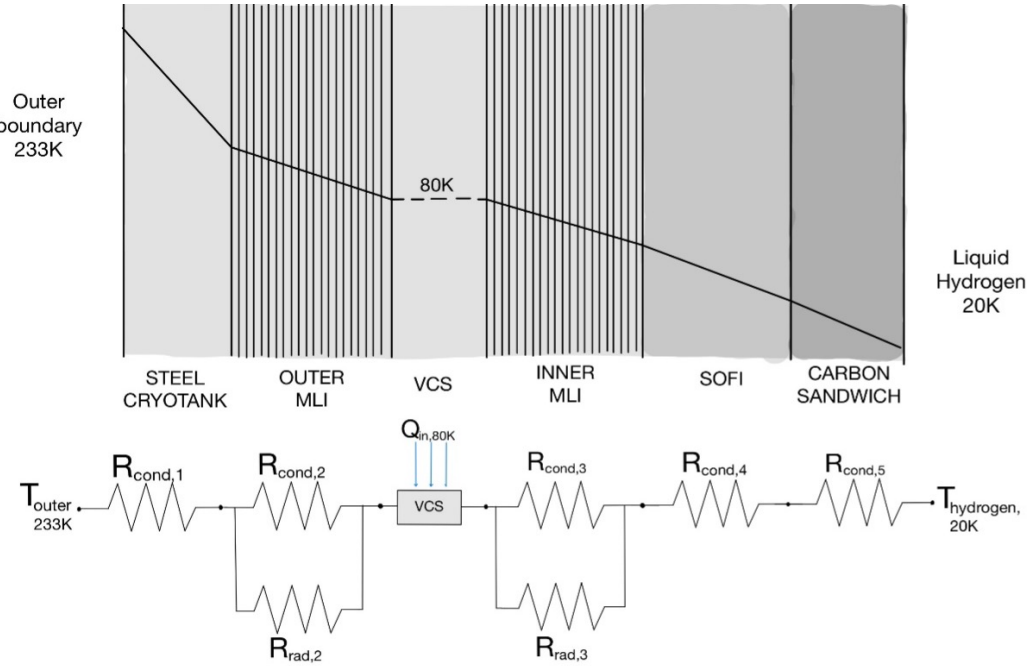


Figure 12: Thermal modelling approach for insulation system [17]

Steel Cryogenic Tank

The use of vacuum insulated vessels for cryogenic liquid storage was first introduced by James Dewar [18]. At its best heat transfer by residual gas is negligible due to the high performance of the vacuum. The entire structure is in a vacuum cryo-tank; resulting in reduced heat flux as there is no convection of air. The thermal conduction resistance is given by

$$R_{cond} = \frac{\Delta x}{\lambda A} \quad (7)$$

where x is the steel thickness, A is the surface area and λ is the thermal conductivity. Therefore, the thermal resistance for the steel section of the cryo-tank is calculated as 9.0×10^{-6} K/W. As expected, this gives the lowest thermal resistance, resulting in the highest contribution to heat flow.

Table 3: Values used in equation (6) to determine Q_{hf}

Material	Thermal Conductivity (W/mK)	Emissivity	Surface Area (m ²)	R _{rad} (K/W)	R _{cond} (K/W)
Steel Cryotank	13.5		35.06		9.0 ×10 ⁻⁶
MLI outer	25	0.0125	32.67	1.27	0.65
MLI inner	25	0.0125	32.67	55.34	1.4
SOFI	24.4		31.51		0.12
Carbon outer	1.07		31.45		1.4 ×10 ⁻⁶
Honeycomb core	2.14		3.1.4		1.5 ×10 ⁻⁶
Carbon inner	1.07		31.3		3.8 ×10 ⁻³

Multi-Layer Insulation with Vapour Cooled Shield

To reduce the heat load on the liquid hydrogen, heat interception through a vapour cooled shield (VCS) is used to maintain an intermediate constant temperature of 80 K. The VCS is actively cooled by hydrogen boil-off which is vented through a network of cooling tubes welded to the steel, embedded in the MLI as shown in Figure 13. This provides distributed cooling to the steel shell as shown in Figure 14. The cooling system consists of a cryocooler namely the Reverse Turbo Brayton Cycle, in addition to a fan used as a circulator and the reservoir which prevents excessive pressure when the system is warm. The VCS significantly reduces the heat flow into tank by 64.3 %, from 1110 W to 396 W.

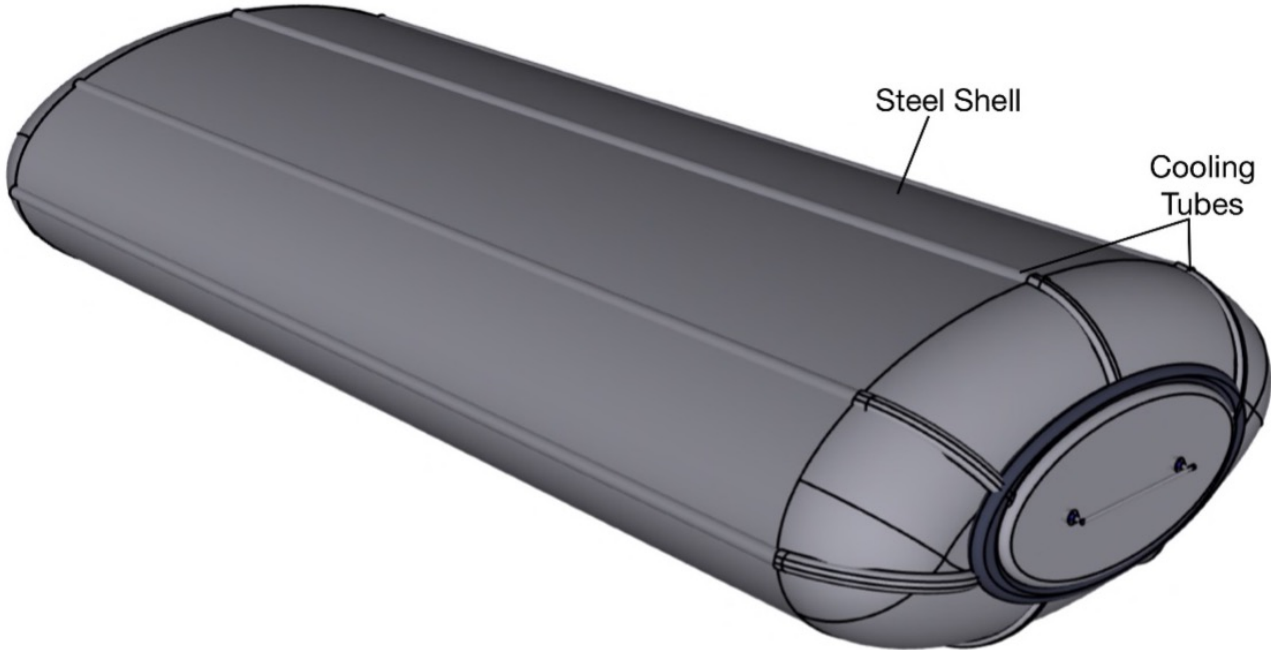


Figure 13: Vapour Cooled Shield

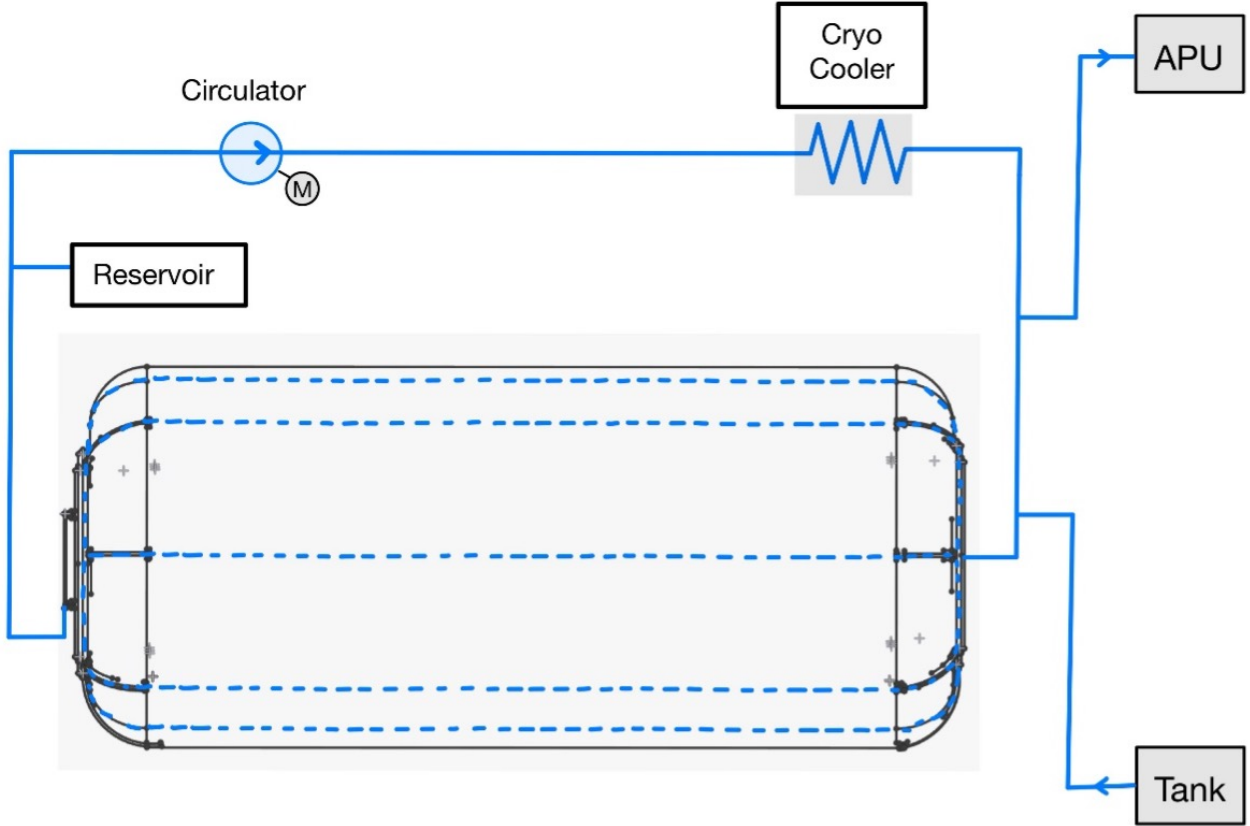


Figure 14: Vapour Cooled Shield cooling system diagram

The MLI comprises of layers of double-aluminized mylar (DAM), alternating with a Dacron net. The configuration consists of 25 internal reflectors and a layer density of 11 layers/cm [19]; with the optimal layer density derived from Figure 15 provided as a result of tests conducted by the University of Washington [19]. The DAM acts as a radiation shield; causing radiation to be reflected from the surface; whilst the Dacron net acts as a low conductivity spacer, preventing additional heat transfer between the layers on Mylar themselves. These two factors are considered when calculating the total thermal resistance; giving a modified equation incorporating radiation and conductivity effects. These are added in parallel as per the heat transfer model in Figure 12 to give the MLI contribution to heat transfer. The emissivity (ϵ_m) of the MLI is calculated as shown in equation (8) using boundary temperatures T_h and T_c . The radiation thermal resistance can be calculated as shown in equation (9) [20], using this value of emissivity.

$$\epsilon_m = 1.18 \times 10^{-2} + 6.18 \times 10^{-5} \frac{(T_h + T_c)}{2} \quad (8)$$

$$R_{rad} = \frac{1}{\epsilon \sigma_{SB} A (T_s^2 + T_{surr}^2)(T_s + T_{surr})} \quad (9)$$

σ_{SB} is the Stefan Boltzmann constant and T_s and T_{surr} are the hot and cold boundary temperatures of the MLI.

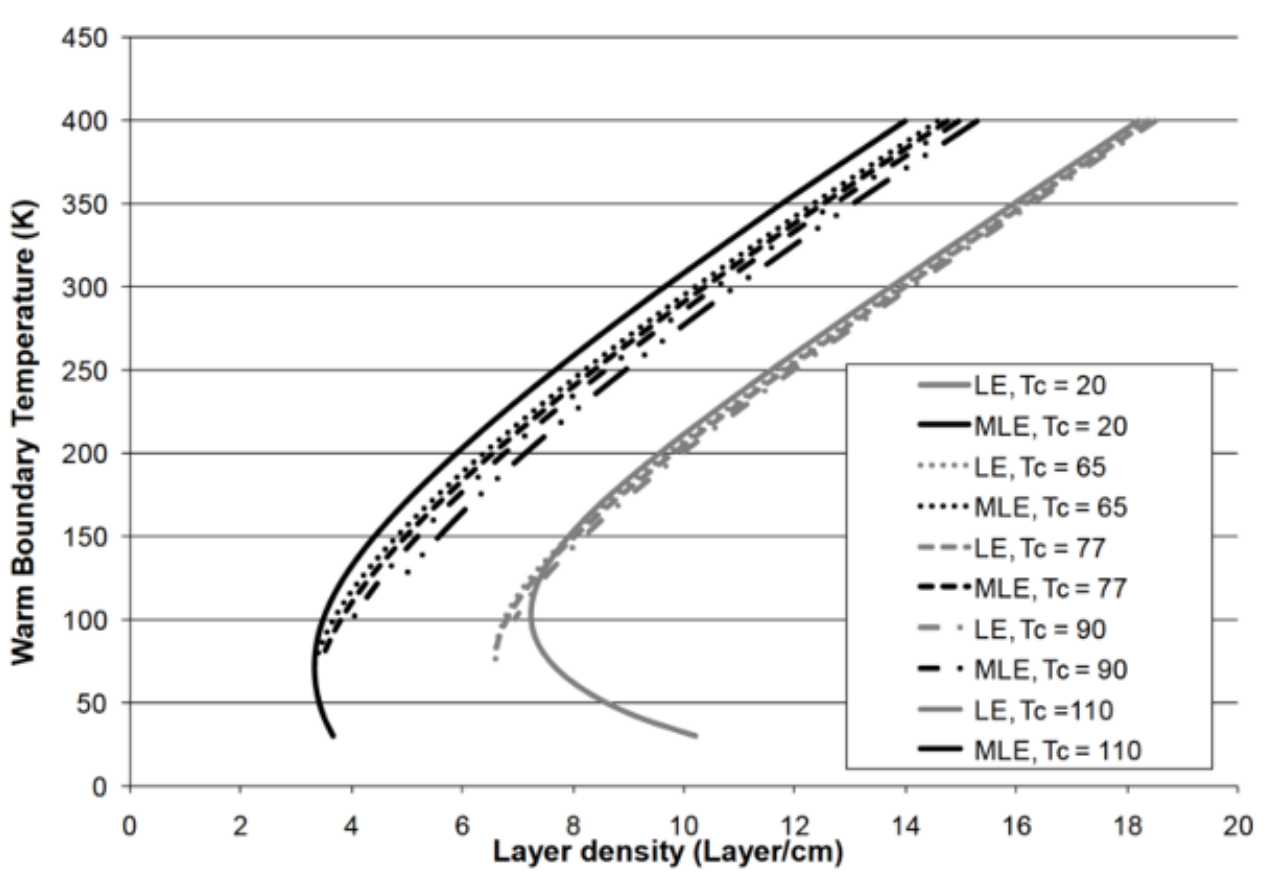


Figure 15: Optimal MLI Layer Densities for Double Aluminized Mylar and Dacron Net [19]

Spray on Foam

Spray on foam insulation, specifically North Carolina Insulation Foam (NCI27-68), is used between the aluminium liner and MLI inner layer. It is applied by spraying it directly on the outer shell of the tank to 24.4 mm. The foam provides a closed cell barrier, and its thermal resistance of solid conduction is calculated with equation (8) as 0.12 W/K; where the thermal conductivity is given by the function in equation (11) where T_f is the average temperature of the foam estimated as 50 K.

$$\lambda_F = 0.88 \times 10^{-3} + 1.92 \times 10^{-4}(T_f - 20) \quad (10)$$

Honeycomb Sandwich

One of the main concerns for calculating heat flux through the honeycomb sandwich panels is the air gaps present in the structure. According to J.J. Darji's study on honeycomb sandwich [21], the effect of convection heat transfer of air inside the honeycomb sandwich can be ignored, simplifying the calculations needed. Therefore, the thermal resistance of the honeycomb sandwich gives a value of 3.8×10^{-3} W/K.

3.4.5 LH2 Crossfeed System

Transfer of fuel between tanks is required for several reasons. Firstly, if there is a fault with one engine, the fuel can be transferred across to the other tank which supplies fuel to the other engine. Secondly, the redistribution of fuel improves the longitudinal balance of the aircraft when in flight and refuelling. A schematic shown in Figure 16 illustrates two pipes which transfer fuel in the designated direction. Depending on the level sensor readings for each tank, the boost pump attached to the tank with less fuel will be turned off. Next, the two shut-off valves on each end of the pipe open and fuel will be pumped at 1 KPa higher than the operating pressure of the tank with less fuel to create a pressure differential. Once the fuel in both tanks are level, the crossfeed pump will turn off ,

the shut-off valves close and the boost pump turns on again. A pipe diameter of 10 cm was required in order to ensure low turbulence and low vapour volume fraction in the transfer lines.

3.4.6 Tank Venting System

In conventional aircraft, when fueling or de-fueling, air must be fed into or out of the fuel tanks in order to maintain tank pressure. This prevents tanks from rupturing, by explosion or implosion, by balancing the inner tank and ambient pressure. Although the purpose of a vent system for liquid hydrogen is the same, when designing a liquid hydrogen fuel tank venting system there are more issues to consider than with conventional fuel. Due to the extremely low temperatures required to store LH₂ fuel, the vent system must not let ambient air enter the tank. This is to minimise any heat transfer from the air into the tanks, prevent any contaminants from entering the system and prevent the freezing of air at any point within the system. Liquid air freezes at a temperature of 58 K, which is considerably higher than the temperature within the tanks of approximately 20 K.

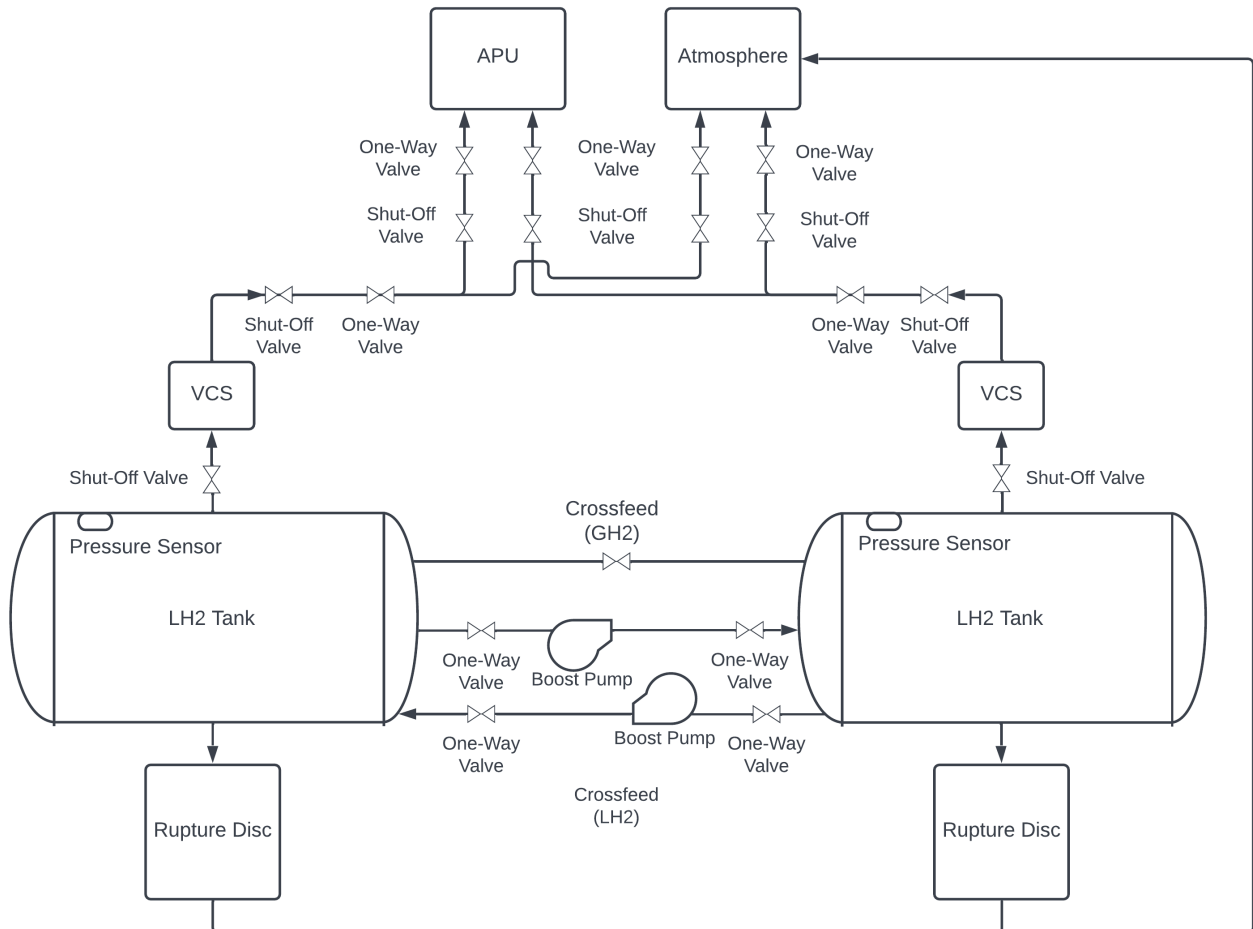


Figure 16: Schematic Diagram of Tank Venting system

When selecting the tank vent pressure, it is important to consider the trade off between tank weight and rate of boil-off. A thicker tank will have a higher mass, however will be able to withstand a higher pressure within the tank, minimising boil-off. Weight minimisation is a priority in aviation and as a result, the tank vent pressure was chosen to be 1.4 bar. Pressure sensors situated within the tanks monitor the internal tank pressure. Once this pressure exceeds a predetermined vent pressure of 1.4 bar, shut-off valves are opened automatically to let excess gaseous hydrogen leave. This ensures that the internal pressure is always below 1.4 bar, protecting the tanks. Following all shut-off valves is a one way valve, ensuring that there is no back flow through the system. After leaving the tanks, gaseous hydrogen boil-off can follow two routes. The first of which is to the APU where it can be used to generate electricity to power electrical systems within the aircraft. The second route is via an exhaust

outlet to the atmosphere. A hydrogen/air mixture is formed at the exhaust outlet of the venting system, which is flammable. Therefore, the exhaust outlets are placed at the end of the wings so that they are far from any heat source, such as the engines. However, the outlet cannot be placed at the wingtip as this area is most susceptible to lightning strikes shown in Figure 17. Flame arresters are also installed at the outlet to protect the fuel system. These devices prevent external fire source from entering the system while allowing ventilation of fuel vapour [22]. One-way valves are also incorporated here to ensure that no air from the atmosphere can enter the fuel system.

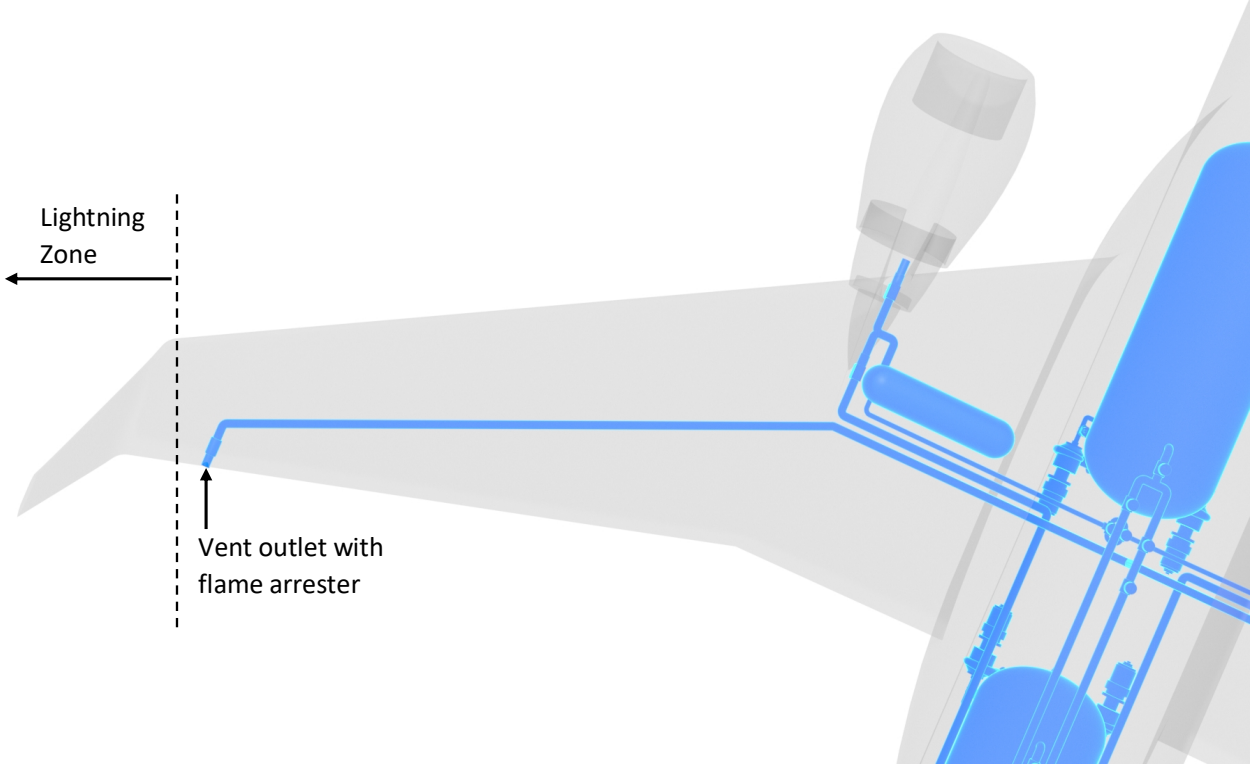


Figure 17: Lightning zone at wing tip [22]

Each tank has its own venting valves which then join the same pipelines to the APU or the exhaust outlets. If the venting system of one tank fails, cross-feed between the tanks ensures that both tanks can still be vented. In the unlikely case that both venting systems fail in a way such that gaseous hydrogen cannot be vented out of the tank after exceeding the venting pressure, each tank is equipped with an emergency non-reclosing pressure relief safety device. This device is a rupture disc consisting of a one-time-use membrane that bursts when a predetermined differential pressure, of 1.35 ± 0.15 bar is reached. This device is connected to the exhaust outlets allowing GH₂ to escape the tank in a controlled manner rather than damaging or bursting the tank which could cause damage to the aircraft structure.

The shut-off valves of the venting system are chosen to be solenoid operated rather than motor operated. Whilst a motor operated valve stays in the last commanded position, solenoid operated valves can be configured to fully open when de-energised. This is a significant advantage of solenoid operated valves as in case of an emergency, such as electrical power failure, excess hydrogen boil off can still leave the tanks to prevent damage to the fuel system [23].

Venting System Electronics

The electronic control of the tank venting system is depicted in Figure 18. Pressure sensors monitor the internal pressure of the tanks and return data to the microcontroller through an ADC (Analog to Digital Converter). The microcontroller processes this data to determine the position of the shut-off valves. If the internal pressure is larger than 1.4 bar, the shut-off valves will be opened. Once pressure drops below 1.35 bar, shut-off valves will be closed. There is a 0.05 bar difference between the positions of the valves to create hysteresis. This protects the valves and ensures that the switching behaviour of the valves is stable. An actuator circuit is needed as a current amplifying

circuit because the solenoid shut-off valves require high current to operate while the microcontroller works on low current signals. This device increases the current from the microcontroller so that valves receive enough power. In addition, the pilot can also gain control over the valves with switches installed inside the cockpit.

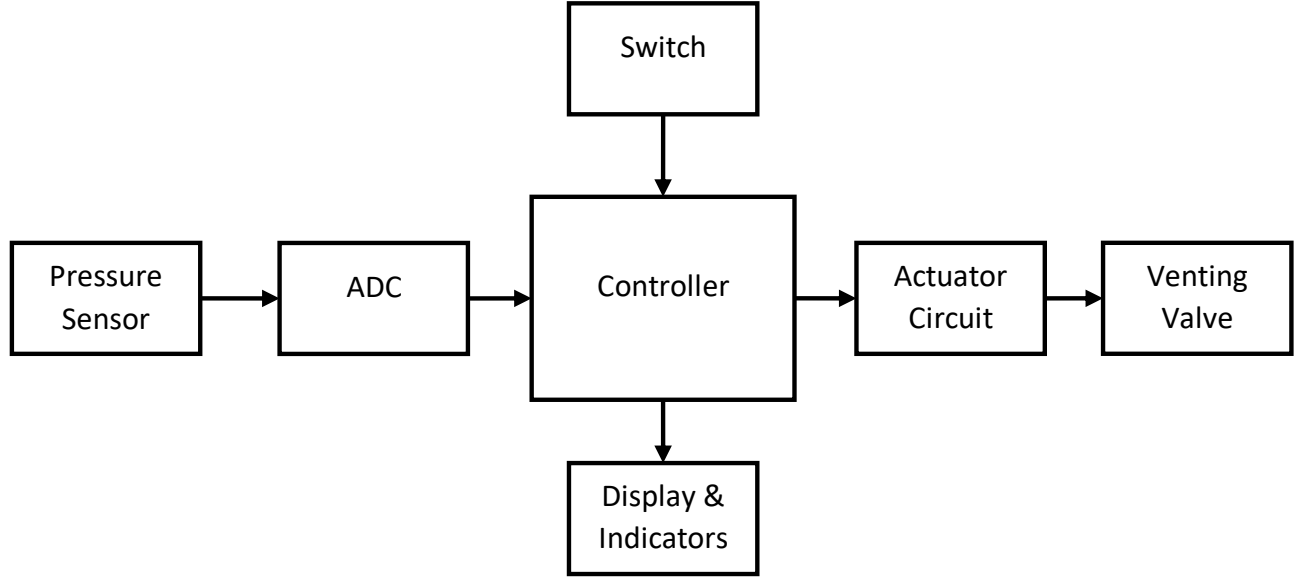


Figure 18: Electronics of Venting Control System

3.4.7 Pressure Generation System

As the fuel level of LH₂ decreases throughout the duration of the flight, the volume of GH₂ in the tank will increase, reducing the pressure within the tank. The pressure within the tank must not fall below the vapour pressure of hydrogen, 0.9 bar, (refer to section 3.5.4) or the atmospheric pressure. Gently heating the LH₂ within the tank causes a small volume of hydrogen to boil-off, increasing the pressure within the tank. This is achieved using a small heating coil placed inside the tank. Constantan was selected for the material of this coil due to its low thermal variation of resistivity and high resistivity. Based on the maximum mass flow rate, a maximum conversion rate of LH₂ to GH₂ was calculated. The energy required to perform this conversion was then calculated as 400 W using the values for the latent heat of vaporisation (476 kJ/kg) and specific heat capacity of hydrogen (14.3 J/gK). A working voltage of 1 kV was chosen. The required current according to equation (11) is therefore 400 mA. The required resistance can then be calculated using equation (12) which can be used to calculate the length of constantan wire required (2.26).

$$P_{elec} = V_{volts} I \quad (11)$$

$$R = \frac{I^2}{P} \quad (12)$$

$$R = \rho \frac{L}{A} \quad (13)$$

3.4.8 Tank Level Sensing

A hydrostatic level sensor was chosen over any chemical or capacitive methods due to its simplicity. The hydrostatic level sensor works on the following principle. When liquid is stored in a vessel, it exerts a hydrostatic force (P_h) on the bottom of the vessel. Thus, as the level of liquid hydrogen decreases (h), the hydrostatic force exerted on the bottom of the tank decreases, according to equation (14).

$$P_h = \rho g h \quad (14)$$

This change in hydrostatic force is measured by the sensor, which outputs a small voltage. This voltage is then amplified and processed where it is then used to display information to the pilot and as an input for the many negative feedback systems present in the fuel system.

3.4.9 Tank Temperature and Pressure

Pressure sensing in our system is achieved via the use of thin film cryogenic pressure transducers placed in every segment of our pipes and in our tanks. These sensors are different to the leak detection pressure transducers mentioned in section 3.5.3. These provide diagnostics to the pilot and computer system allowing for automatic adjustments and manual override. For measuring temperature, a Pt-100 Platinum temperature sensor is used, with a 4-wire connection for increased accuracy. These are placed at regular intervals throughout the fuel system.

3.4.10 Fuelling and Defuelling

Currently the E190 can refuel for a flight in 10 minutes. An E190 retrofitted with this hydrogen fuel system should have a similar refuelling time to ensure operating an aircraft with this fuel system is economically viable and feasible on a busy airport apron. In order to refuel the E190 with 1100 kg of LH₂ in 10 minutes the mass flow rate required is 1.83 kg/s and so the volumetric flow rate is 0.026 m³/s. Equation (15) shows the relationship between volumetric flow rate (Q), pipe cross sectional area (A) and flow speed (v). There is an important trade off to be made between keeping the flow speed and cross-sectional area low. Low flow speeds mean less turbulent flow in the pipe and reduced boil off losses. However, a low cross-sectional area is required to keep the weight of the refuelling hose low for human handling. A pipe diameter of 0.1 m has been chosen which results in a flow speed of 3.3 m/s. The manifold splits into two pipes, supplying both the fore and aft tanks. Since the flow rate halves, the cross-sectional area of the pipe must halve to maintain a speed of 3.3 m/s. The diameter of each manifolded pipe is 0.07m.

$$Q = Av \quad (15)$$

The plane will be fuelled by pressure refuelling, entering the plane on the under belly of the fuselage. The pump on the fueling truck will create the necessary drive to fuel and defuel the tanks without the need for additional pumps on the plane. The fuel system will fill both tanks by means of a manifold connecting to both the tanks from the refuelling hose.

Before refuelling, the tank pressure will be maintained between 1.25 and 1.45 bar by the pressure drop and generation system. During refuelling as LH₂ enters the tank, the volume for GH₂ will decrease and so pressure will increase. Equation (16) is used to derive equation (17) at constant temperature and mass of hydrogen. Equation (17) can then be used to determine that after refuelling, the pressure in the tank would reach 35.6 bar without any venting. This high pressure risks bursting the tank. Therefore, the venting system must be used during the fuelling process to release some GH₂ and to maintain a pressure below 1.448 bar inside the tank.

The ideal gas law (16) is used here to demonstrate the change of pressure with changing volumes of gas. The pressure values calculated assume an ideal gas occupies the tank. However, GH₂ at temperatures just above its boiling point is not an ideal gas and so these numerical values are only used to demonstrate the increase and decrease of pressure and not specific values.

$$PV = mRT \quad (16)$$

$$P_1 \times V_1 = P_2 \times V_2 \quad (17)$$

There must be some element of control when refuelling the tanks because it is likely the fuel levels in each tank will not be equal. Control is needed to fill the tanks at appropriate rates so that they will both have the same volume of fuel after refuelling and so that fuel is not forced into an already full tank. Forcing fuel into a full tank would result in large pressures pushing out on the tank wall, which risks bursting the tank. Refuelling positioning control can be achieved by two methods. Firstly, fuelling the tanks at the same volumetric rate and using the cross-feed monitoring system to move and distribute the fuel equally between the two tanks. The second method is to have a manual controller working a mechanical valve system that can feed the tanks individually and simultaneously. Refuelling personnel will monitor the displays of the fuel levels and choose where to direct the fuel with valve control switches. By closing a tanks valve and opening the other tanks valve the controller can fill a tank individually and when the fuel levels are equal they can open both valves to fuel the tank simultaneously.

The second method of manually refuelling has been chosen in the fuel system as opposed to the cross-feed feedback system. Passing the LH₂ unnecessarily across the cross-feed pipes would result in additional unwanted boil-off due to the pipes large surface area to volume ratio. Having a manually operated refuelling system directs the fuel straight to the tanks without having to send the fuel further than necessary.

Defuelling of the plane tanks may be necessary for maintenance checks within the tanks. When defuelling the pressure in the tank will decrease as the GH₂ will occupy more volume. Using equation (17) it is calculated that without any pressure generation the tank pressure will drop to 0.04 bar risking tank implosion. To overcome this, there is pressure generation system within the tank. Whilst defuelling, the system carefully heats the LH₂ within the tanks to generate up to 32.6 kg of GH₂, to maintain a pressure above 1.2 bar.

Spark Risk

Plane infrastructure today has many existing precautions to prevent spark risks when refuelling a plane. Sparks must be prevented from jumping between different electrical potentials because they may ignite the explosive hydrogen fuel. Bonding points exist on the plane to connect a bonding cable from the refuelling truck to the plane, preventing electrical discontinuity between vehicles. The plane is also grounded to earth via its tires ensuring electrical continuity between the aircraft and earth.

3.4.11 Tank Cut-outs: Stress Analysis

The cut out for the fuel pipe is at the bottom of the tank and so the fuel can reach the driving pumps positioned below the tanks using gravity feed. Stresses will arise around the tank cut-out due to the tank hoop and axial stresses. Both the fuelling pipe and the engine fuel pipe cut-outs are positioned at the bottom of the tanks. Since the engine fuel pipe has a larger diameter of the two cut-outs, stress analysis was carried out on the refuelling cut-out. The effective radius, $R(\Phi)$, at any point around the ellipse is calculated using equations, where θ is the angle from the major axis of the ellipse. At the bottom of the tank ($\theta = 90^\circ$) and so the effective radius is 0.575 m. The hoop stress (σ_{hoop}) and axial stress (σ_{axial}) of the elliptical tank at the point of the cut-out are 19.45 MPa and 9.73 MPa respectively using equations (20-21).

$$R(\Phi) = \sqrt{b^2 \cos^2 \Phi + a^2 \sin^2 \Phi} \quad (18)$$

$$\tan \theta = \frac{b}{a} \tan \Phi \quad (19)$$

$$\sigma_{hoop} = \frac{P R(\Phi)}{t_w} \quad (20)$$

$$\sigma_{axial} = \frac{P R(\Phi)}{2 t_w} \quad (21)$$

The tangential stresses around the cut-out ($\sigma_{\theta\theta}$) were calculated using equation (22) which models an infinite flat plate subjected to a far field uniaxial stress (σ_∞), used as the hoop and axial stress individually. In equation (22) the far field stress is parallel with $\theta = 0$. The radius of curvature of the ellipse is 2.28 m at the bottom of the tank, calculated using equation (23). Since the radius of curvature is large, the plate is assumed to be flat and that when the pipe makes contact with the curved surface that it will cut a circular hole rather than an elliptically shaped cut out. These two assumptions justify why modelling a circular hole on a flat plate is acceptable here.

Figure 19 shows the resulting stresses around the circular hole due to the hoop and axial stresses and the superposition of these stresses to give the overall stress concentrations around cut-out. The maximum stress around the cut-out due to both the hoop and axial stresses is 48.62 MPa.

$$\sigma_{\theta\theta} = \sigma_\infty (1 - 2 \cos 2\theta) \quad (22)$$

$$R(\theta) = \sqrt{\left(a \cos \theta - \frac{a^2 - b^2}{a} \cos^3 \theta\right)^2 + \left(b \sin \theta - \frac{b^2 - a^2}{b} \sin^3 \theta\right)^2} \quad (23)$$

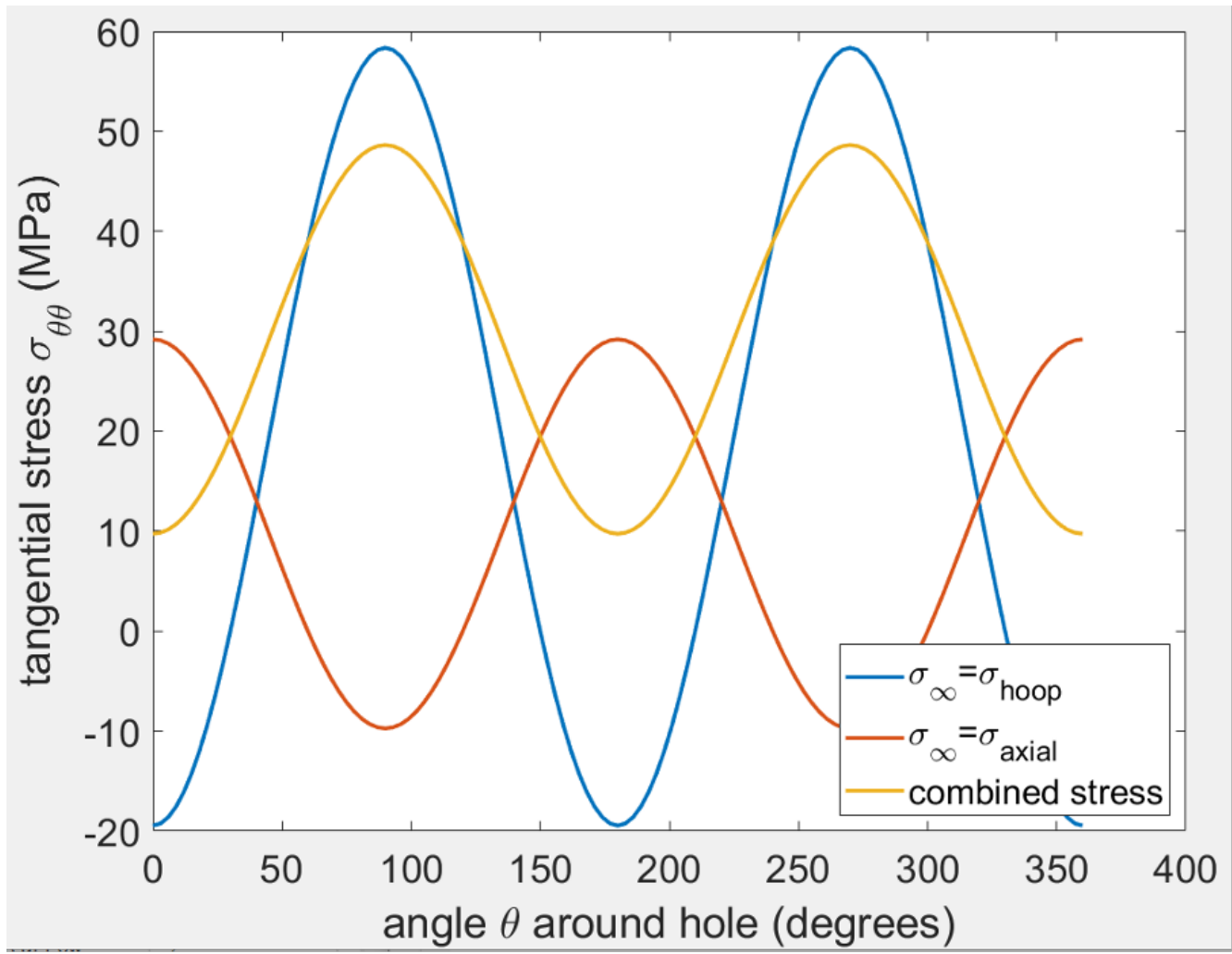


Figure 19: Tangential stresses around fuel pipe cut out due to superposition of the hoop and axial stresses around the tank. $\theta = 0$ is parallel with the axial stress direction, along the axis of the tank.

FEA analysis was used to support the calculations and the analysis results in a maximum stress of 48.9 MPa as shown in Figure 20

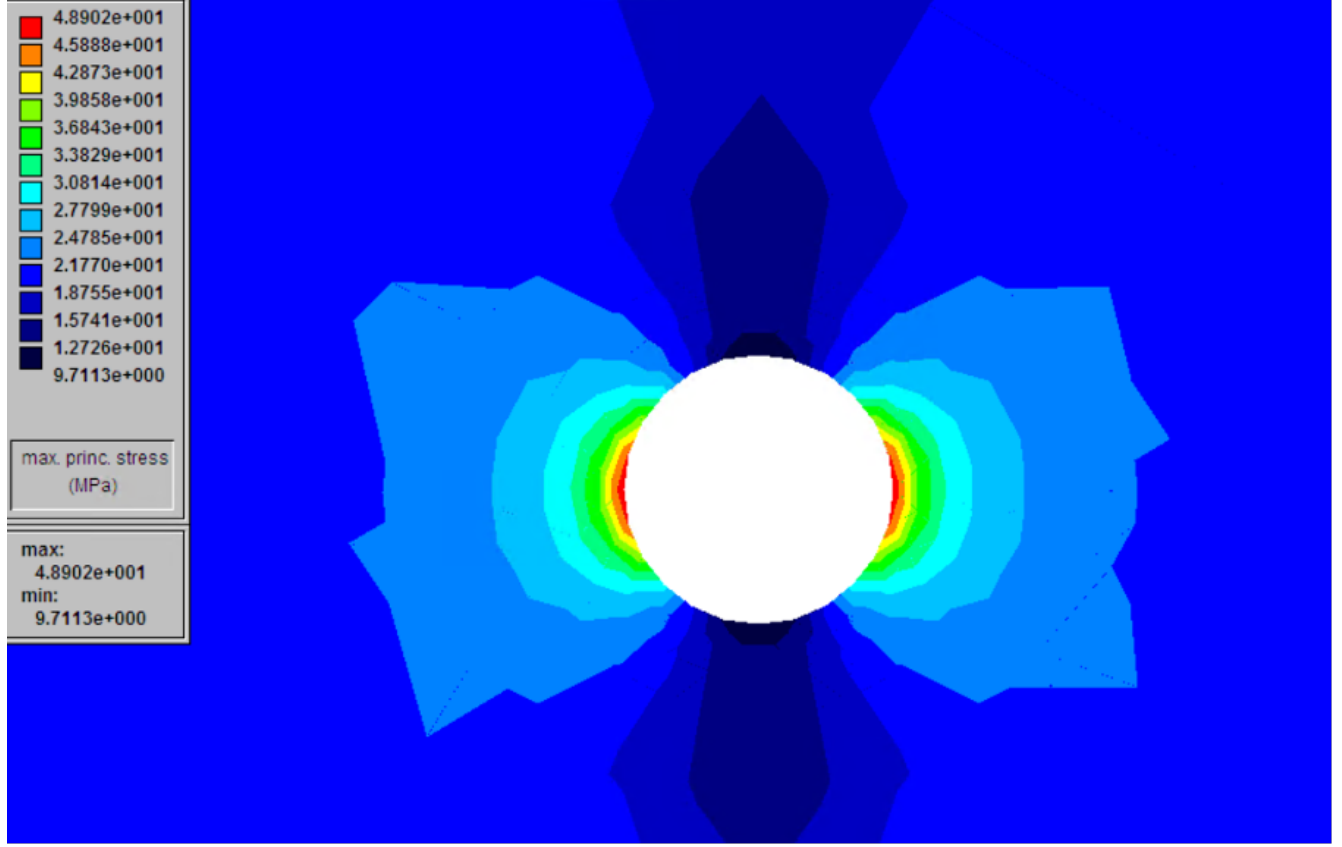


Figure 20: Contour plot showing stress concentration around cut-out

The yield strength of the tank material is 1050 MPa and so using the maximum stress around the hole of 48.62 the factor of safety is calculated to be 21.6. According to [24] pressure vessels in the aviation industry should have a minimum FOS of 6. This is a maximum allowable stress of 175 MPa before having a FOS less than 6. The cut-out for the fuel pipe is a circular hole with diameter 7 cm and in order to assess how large the cut-out size can go before the FOS drops below 6, FEA is required. FEA using Solidworks is required to calculate the stresses around larger sized cut-outs because both the assumptions of modelling a circular hole and a flat plate break down. FEA computes a maximum pipe diameter of 50 cm intersecting the bottom of the tank before 175 MPa is exceeded around the cut-out.

3.4.12 Boil-Off within Tanks

To model boil-off in the tank, a FEA software called BoilFast was used. This software models heat fluxes into vessels and their subsequent actions on the liquid within. Based on previous sections there is a total heat flux into our tank of 500 W. After entering the dimensions of the tank and running the simulation the following results were acquired. For the simulation to run properly a venting pressure of 1.35 bar is selected. Any boil off is immediately vented allowing us to plot the decrease in liquid volume. This is approximately 0.045 m³/hour. This value would be a worst-case scenario as during flight the volume of liquid is decreasing meaning less boil-off is generated as the plane flies. However, the simulation does not account for any motion of the liquid that would be experienced during flight nor does it account for any turbulence created by the flow of hydrogen out of the tank.

3.5 Engine Fuel Delivery

3.5.1 Line Sizing

The engine fuel delivery subsystem was designed to ensure the hydrogen remains as a liquid until it is converted to a gas within the heat exchanger, before entering the engine. The advantage of only using pumps located at the tanks means that a near-zero vapor volume fraction in the pipe is no longer required since it is not being fed into more pumps. However, control of the process is still important. Therefore, maintaining a low vapour fraction is needed which means keeping the volumetric flow rates low to reduce turbulence. This is why LH₂ is converted to gas at the end to accommodate for a 6 fold increase in volumetric flow rate.

The maximum mass fuel flow rate at take-off conditions was used as the design point of the pipeline diameter. Due to commercial competition, engine data is rarely publicly available. Therefore, using the engine datasheet [25], the maximum thrust (F) of the GE CF34-10E engine, 90.6 kN, and specific fuel consumption (SFC), 6.42 g/kNs were used to calculate the maximum mass fuel flow rate (\dot{m}_f) using equation (24). The actual maximum flow rate will be less since the maximum landing mass is used in this design, rather than the maximum take-off mass. The volumetric flow rate calculated using equation (25) was then converted to the energy equivalent fuel mass flow rate for liquid hydrogen. A maximum flow rate was calculated as 0.588 kg/s. In order for the system to handle excess flow, a safety factor of 1.5 was incorporated bringing the maximum flow rate for the fuel system to 0.882 kg/s and this value was used as the design point.

$$SFC = \frac{\dot{m}_f}{F} \quad (24)$$

Pipeline sizing required several design trade-offs. For example, in order to minimise line size weight, the diameter should be as small as possible. However, a smaller diameter increases pressure loss throughout the piping system. Pressure loss disadvantages include increased energy and size requirements for the pump, and also the unpredictability of flow rates associated with an increased pressure drop. Determined by the maximum operating pressure of the engine [26], the maximum exit pressure of the pipe required was 86 bar. At this pressure and an assumed temperature of 20 K, the volumetric flow of LH₂ was calculated as 0.011 m³/s using equation (25).

$$Q = \frac{\dot{m}_f}{\rho} \quad (25)$$

Conventional analysis of incompressible liquid hydrogen in pipes using the maximum flow rate was used. Pressure loss across a range of diameters (d) for the required volumetric flow rate of 0.011 m³/s was investigated using equation (26). The feed line from the tank furthest to the engine (see Figure 21) with a pipe length (L) of 9.5 m, and a growth factor of 1.2 incorporated to account for thermal expansion was used to calculate the maximum pressure loss.

$$\Delta P_{loss} = \frac{u^2 \rho}{2} \left(4f \frac{L}{d} + K \right) \quad (26)$$

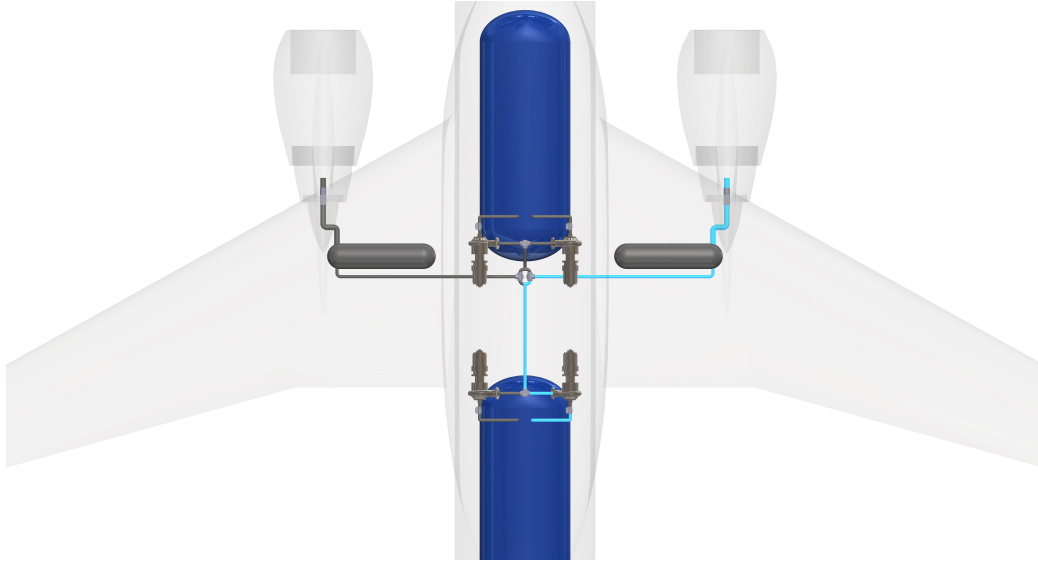


Figure 21: Longest LH₂ route from tank to engine

The K factor values were determined by fittings along the pipeline shown in Table 4. The friction factor (f) was determined by assuming a rough pipe flow with a surface roughness of $3 \mu\text{m}$ [27] and was calculated to vary between 0.0032 and 0.0034 depending on pipeline diameter.

Table 4: Minor loss coefficients of fittings

Fitting	K Factor
Shut-off Valves x2 [23]	3.5
90° bend x5 [28]	5
Check Valve x1 [28]	2
Total	10.5

The results of the pressure drop against LH₂ pipe line diameter are shown in Figure 22. There were minimum limits to the diameter set by the erosional velocity equation which is widely used as a recommended practice in the oil and gas industry. This is to protect the pipe from increased shear stresses for the case of two-phase flow and other effects such as noise and vibration [29]. However, it is recognised there are validity concerns regarding use of equation (27) applied to a hydrogen application. To calculate the maximum erosional velocity (V_e), a 'c' factor of 244 was used for a stainless steel inner pipe [29] and densities of LH₂ as 79 kg/m^3 and GH₂ as 13.05 kg/m^3 . It was recommended to use 50% of the maximum erosional velocity. Therefore, the maximum velocities were calculated as 13.7 m/s and 33 m/s for LH₂ and GH₂ respectively.

$$V_e = \frac{c}{\sqrt{\rho}} \quad (27)$$

These velocities were used as a factor to determine a minimum inner bore diameter of 30 mm and 51 mm for volumetric flow rates of $0.011 \text{ m}^3/\text{s}$ and $0.068 \text{ m}^3/\text{s}$ for LH₂ and GH₂ pipes. The minimum diameter of 30 mm used provided an acceptable pressure loss of 1.4 bar as shown in Figure 22 where the balance between weight and pressure loss is best met for the LH₂ pipe.

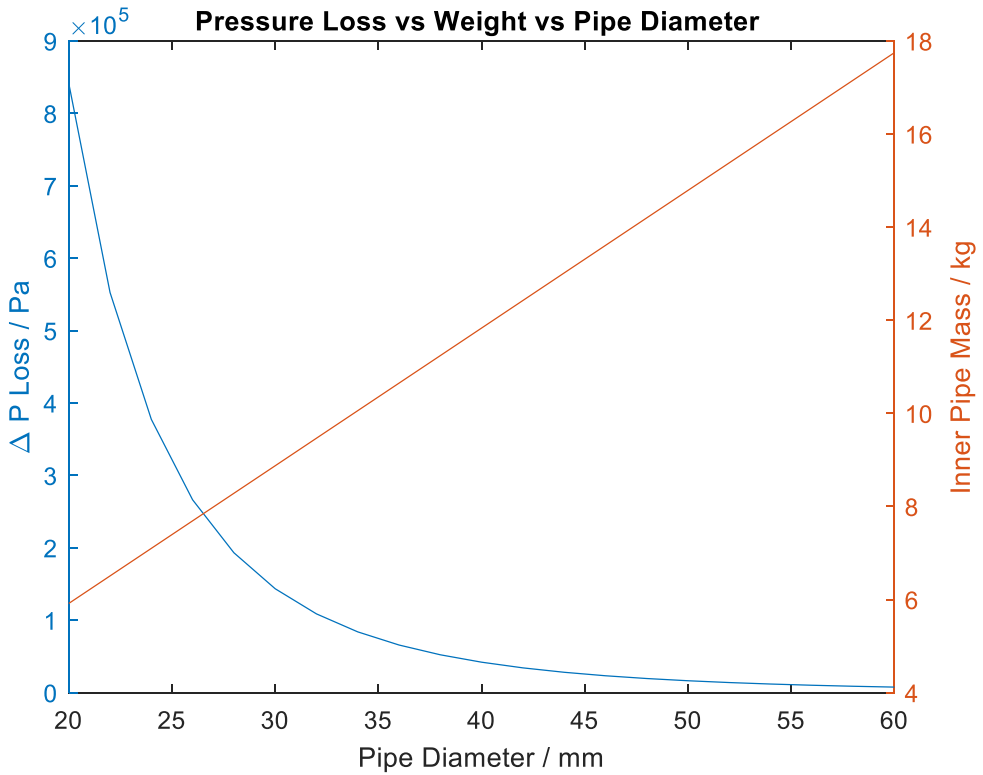


Figure 22: Pressure Loss vs Weight vs Pipe Diameter of LH2 pipe

The thickness of the inner stainless steel (304 series) pipe was determined using equation (28). A maximum working stress was determined as 105 MPa to comply with ISO 2531 standards [30] which states the working stress in the pipe wall must not exceed one-third of the tensile strength or half the yield strength. Using the diameters of the inner bore outlined, and a maximum internal pressure of 87.4 bar, the thickness of the inner steel pipe was calculated as 1.25 mm and 2.1 mm for the liquid and gas phases of the pipe.

$$t = \frac{P_{internal} \times d}{2 \times \sigma_{maxworkingstress}} \quad (28)$$

3.5.2 Pipe Insulation

Shown in Figures 23 and 24, a vacuum jacketed insulation system, similar to the tank insulation, incorporating MLI in the annulus has been selected for use in the pipes. Typical heat flow values for cryogenic pipes are between 1-2 W/m² and so a heat flow (Q) of 1.32 W/m² as per [31] gives an insulation thickness of 17.5 mm for the liquid pipe and 30.5 mm for the gas pipe using equation (29) where L is the length of the pipe, λ is the thermal conductivity of steel, T_o is the outer temperature, T_i is the inner temperature, r_o is the outer radius and r_i is the inner radius (Figure 23-24). Low conductivity copper spacers have been incorporated to keep the inner pipe in place whilst conducting minimal heat energy, as well as bellows which allow for thermal expansion.

$$Q = \frac{-2\pi\lambda L(T_o - T_i)}{\ln r_o - r_i} \quad (29)$$

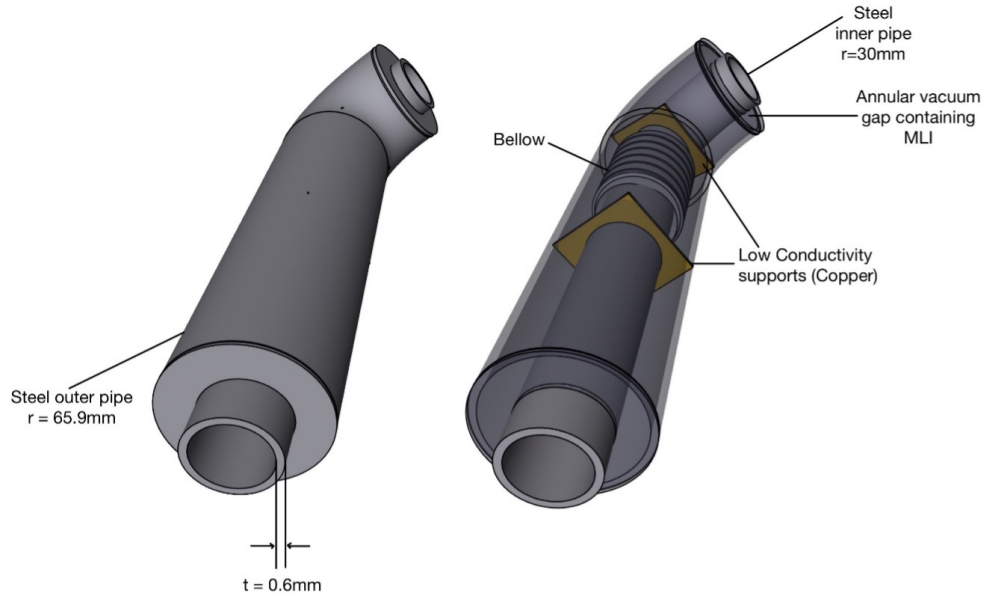


Figure 23: Liquid pipe with inner section view

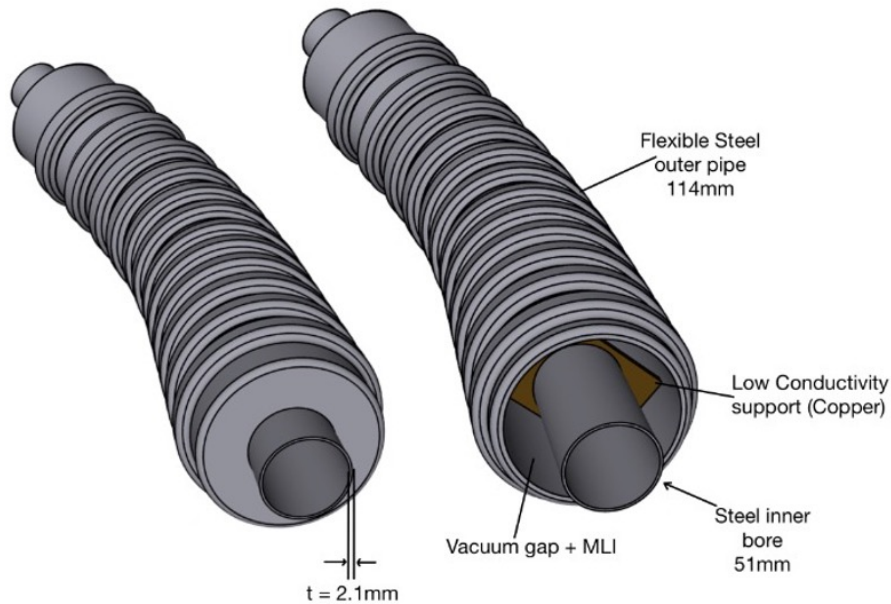


Figure 24: Gas pipe with inner section view

Table 5: Values used to determine heat flow (Q) in equation (29)

Parameter	Value
λ	13.5 W/m ² K
T_o	233 K
T_i	20 K

3.5.3 Heat Exchanger

Before delivery to the aircraft engine, the liquid hydrogen must be gasified and brought to an appropriate temperature for combustion. Unlike conventional aviation fuel, hydrogen does not have a flash point and will ignite at temperatures above its boiling point of 20 K. In conventional gas engines, fuel is injected into the combustion chamber where it is mixed with air and burned. Liquid air has a boiling point of 78.8 K, in between that of nitrogen (77 K) and oxygen (90 K) [32], the two primary constituents of air. The boiling point of air gives a minimum temperature of hydrogen that should be delivered to the engines.

There are several types of heat exchanger design. Although a finned tube heat exchanger was considered, a U-Tube heat exchanger was selected as the most appropriate for the fuel system as its tubular shape allowed for greater flexibility in the positioning of the heat exchanger. The fuel system incorporates two heat exchangers situated towards the base of the wing occupying space that is filled by the fuel tanks in conventional fuel systems. Each heat exchanger is primarily fashioned out of Aluminium 2219-T87. Aluminium alloys are widely used in cryogenic applications as they demonstrate a good relationship between strength and fracture toughness, with only small changes to their material properties at these extreme low temperatures [33]. This particular alloy of aluminium has been used in several other systems handling liquid hydrogen and has been praised for its weld-ability [34].

The shell side fluid was chosen to be ambient air. This choice was made to take advantage of the large temperature difference between liquid hydrogen and an aircraft's surroundings, and eliminates the need for an additional fluid system onboard the aircraft. In addition, other shell side fluids that may be liquid at room temperature and pressure have much higher freezing points. In order to ensure they do not begin to solidify within the heat exchanger, the thickness of the tubeside pipes would have to increase to raise the outer tubeside surface temperature. The overall mass of the heat exchanger would therefore be greater.

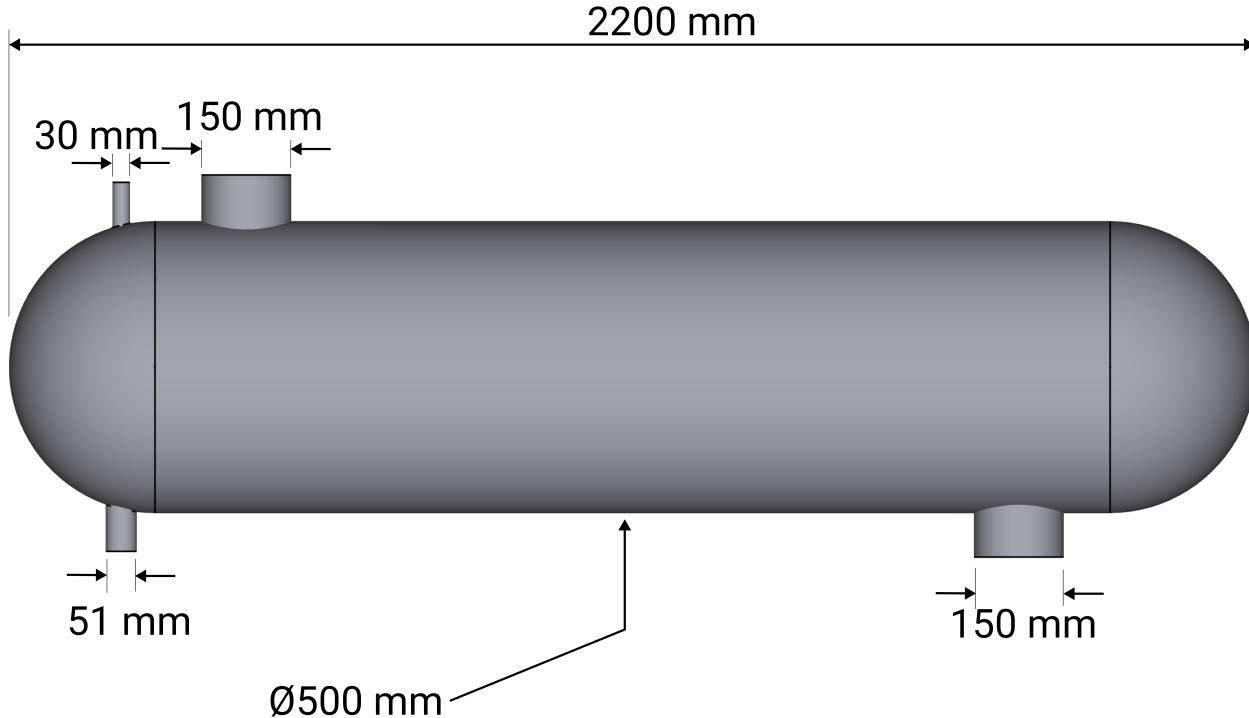


Figure 25: Heat Exchanger Dimensions

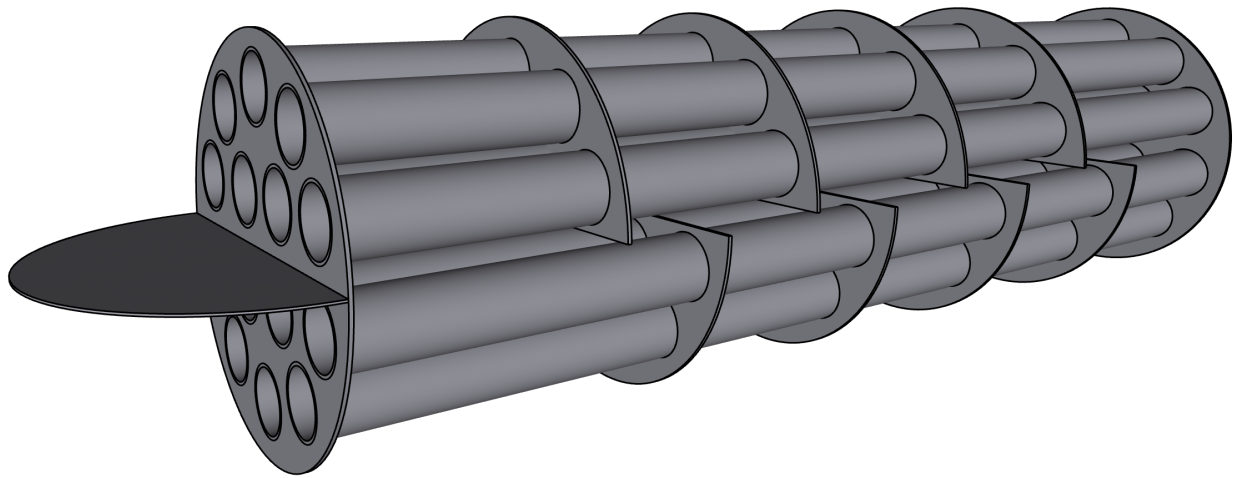


Figure 26: Heat Exchanger Tubeside

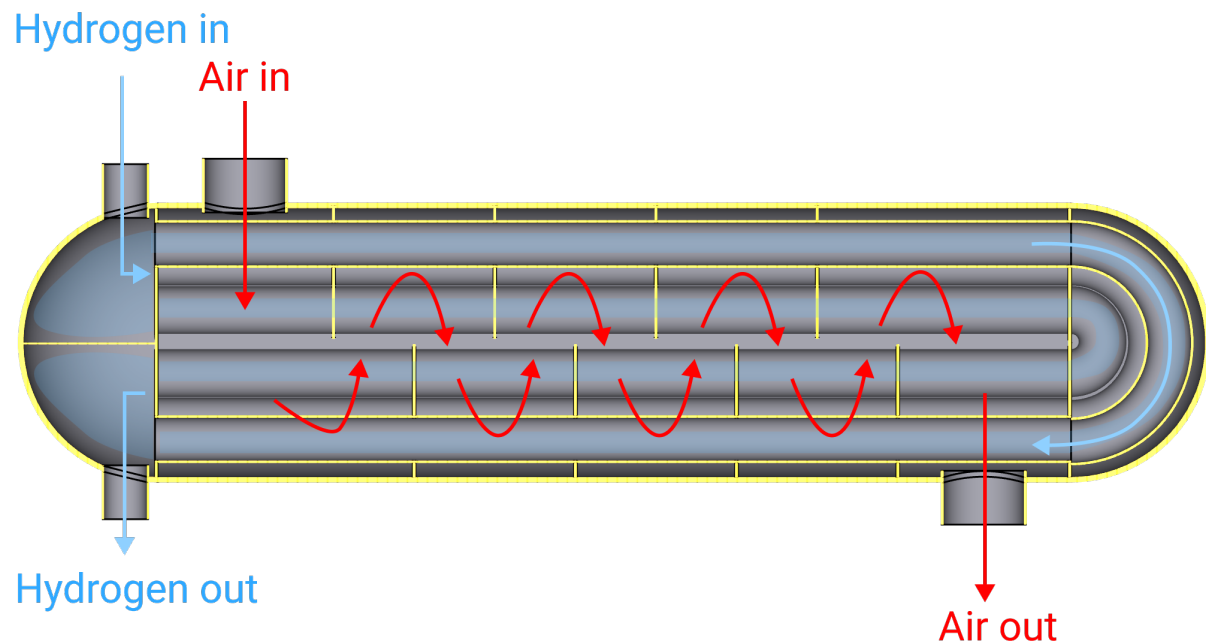


Figure 27: Flow through heat exchanger

Table 6: Heat Exchanger Dimensions

Dimension	Value
Required Air Intake Area	0.25 m ²
Shell Side Inlet/Outlet Diameter	150 mm
Tube Side Inlet Diameter	30 mm
Tube Side Outlet Diameter	51 mm
Heat Transfer Area	6 m ²
Diameter	500 mm
Length	2.2 m
Tube Length	1.7 m
Number of Tubes	7
Number of Tube Passes	2
Baffle Spacing	150 mm

Heat Exchanger: Sizing

In order to size the heat exchanger, the NTU (Number of Transfer Units) method was used as only the inlet temperatures of the heat exchanger were known [35]. The method used to size the heat exchanger can be broken down into the following steps:

1. Determine the effectiveness of the heat exchanger:

The effectiveness of a heat exchanger (ϵ) is a ratio relating the actual rate of heat transfer to the maximum rate of heat transfer that could be achieved and can be found using the following equation

$$\epsilon = \frac{C_c(T_{c,o} - T_{c,i})}{C_{min}(T_{h,i} - T_{c,i})} \quad (30)$$

where C_c is the heat capacity rates for the cold fluid, C_{min} is the lowest of the two heat transfer rates for the hot and cold fluid, $T_{c,o}$ and $T_{c,i}$ are the outlet and inlet cold fluid temperatures and $T_{h,i}$ is the hot fluid outlet temperature. In this case, the hot fluid is ambient air and the cold fluid is the hydrogen flowing through the tube side of the heat exchanger. The following equations

$$C_c = \dot{m}_{H_2} c_{p,H_2} \quad \text{and} \quad C_h = \dot{m}_{air} c_{p,air} \quad (31)$$

can be used to determine the heat capacity rates for both fluids.

2. Determine the number of transfer units:

The dimensionless number of transfer units can be found using the following equations

$$NTU = -\frac{\ln \frac{E-1}{E+1}}{(1 + (C_r)^2)^{1/2}} \quad (32)$$

$$E = \frac{2/\epsilon - (1 + C_r)}{(1 + (C_r)^2)^{1/2}} \quad (33)$$

where C_r is the heat capacity ratio (C_{min}/C_{max}) and E is a function of the effectiveness of the heat exchanger.

3. Find the overall heat transfer coefficient (U):

In order to determine the overall heat transfer coefficient, it is first necessary to determine the convection heat transfer coefficients for both the tube and shell side fluid [36]. The convection heat transfer coefficients h_{H_2} and h_{air} can be found by following the procedure detailed in equations (34 - 37).

$$(Tubeside) \quad Re = \frac{4\dot{m}}{\pi D_i \mu} \quad \text{or} \quad Re = \frac{4\dot{m}}{\pi D_o \mu} \quad (Shellside) \quad (34)$$

$$Pr = \frac{\mu c}{\lambda} \quad (35)$$

$$(Tubeside) \quad Nu = 0.023Re^{0.8}Pr^{0.33} \quad \text{or} \quad Nu = 0.196Re^{0.6}Pr^{0.33} \quad (Shellside) \quad (36)$$

$$h = \frac{Nu \lambda}{D_{i,o}} \quad (37)$$

The overall heat transfer coefficient, U , can then be calculated using the following equation

$$U = \left(\frac{1}{h_{air}} + \frac{x_{al}}{\lambda_{al}} + \frac{1}{h_{h_2}} \right)^{-1} \quad (38)$$

4. Determine the heat transfer surface area of the heat exchanger:

$$A = NTU \times \frac{C_{min}}{U} \quad (39)$$

Following the above procedure gives a required heat transfer surface of 2.11 m^2 . The heat transfer area of the heat exchanger designed is 6 m^2 , giving a FOS of 2.84. Table 7 lists the values used in the calculation.

Using data on the physical properties of air at increasing elevation [37], it is possible to demonstrate the performance of the heat exchanger in a range of expected operating conditions.

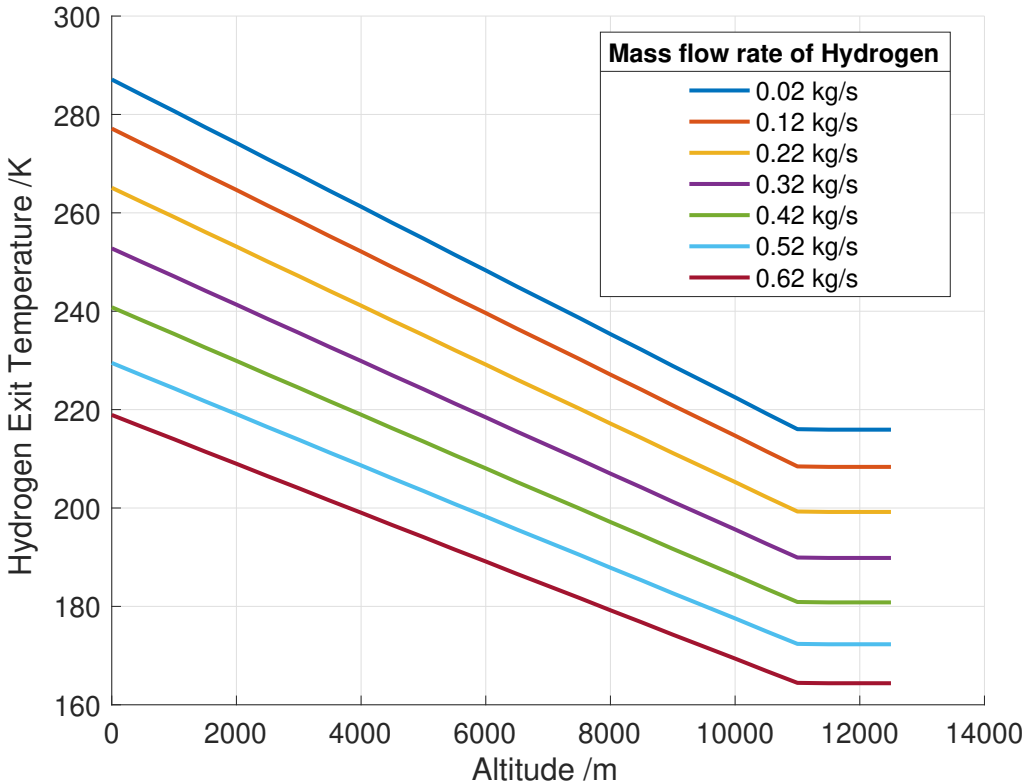


Figure 28: Hydrogen Exit Temperature from heat exchanger at increasing mass flow rates of hydrogen. (Air mass flow rate = 3 kg/s)

As shown in Figure 28, as the plane climbs, the hydrogen exit temperature decreases until the plane reaches an elevation of around 11 km. This is expected given the changes to the ambient air temperature the plane increases in altitude. In the troposphere (lowest region of the atmosphere) there is a negative linear relationship between temperature and altitude, however at 11 km, there is a region of relatively constant temperature, called the tropopause [38]. Figure 28 also shows that as the mass flow rate of hydrogen increases, the exit temperature of the hydrogen decreases. The maximum and minimum hydrogen flow rates through the system of 0.588 kg/s and 0.14 kg/s occur at take-off and cruising respectively.

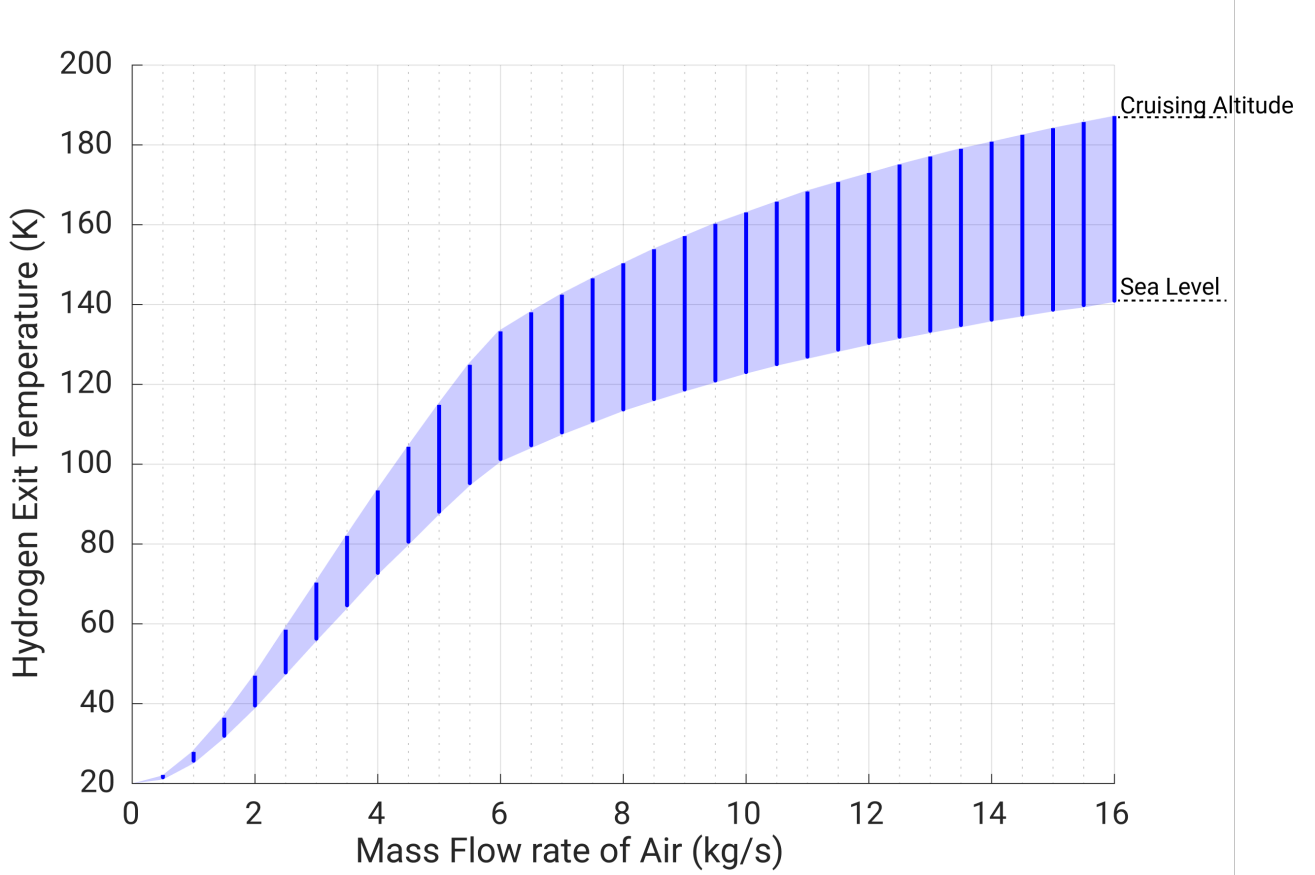


Figure 29: Hydrogen exit temperature from heat exchanger at increasing air mass flow rates in the shell side of the heat exchanger [37]. Hydrogen mass flow rate = 0.588 kg/s.

In order to deliver hydrogen to the engines at an appropriate temperature when the aircraft is stationary, or taxiing an axial fan is required before the ambient air inlet to the heat exchanger. Figure 29 shows that an increase in the mass flow rate of air relates to an increase in the hydrogen exit temperature. The corresponding hydrogen mass flow rate in Figure 29 is the take-off flow rate. This is when the flow rate of hydrogen should be greatest. Using Figure 29 it can be determined that the axial fan must be able to drive a minimum mass air mass flow rate of no less than 6 kg/s through the shell side of the heat exchanger. This would deliver hydrogen to the engines at 100 K (20 K above the minimum temperature 78.8 K determined earlier) as the aircraft is beginning to accelerate down the runway. With an air intake area of 0.25 m^2 , this mass flow rate of air is achieved at a speed of 19.6 m/s. With a take-off speed (V_2) of 135 kts or 69.45 m/s [39], the fan will only be required during the early stages of take-off, when the aircraft is travelling at a speed below 19.6 m/s.

Heat Exchanger: Assumptions and Design Limitations

There are various assumptions associated with the NTU method. These include the assumption that the flow is fully developed and in a steady state, fluid and material properties are constant, there are no losses to the surroundings and the fluid is unmixed on both sides. Due to the nature of the heat exchanger, several physical properties of the tube side and shell side fluid are variable and therefore, in particular, this assumption of the method is violated.

For example, the dynamic viscosity of hydrogen changes with temperature. In this instance, a dynamic viscosity corresponding to an intermediate temperature of hydrogen in the heat exchanger was selected. This approach was applied where necessary, with values used listed in Table (6). Furthermore, the method does not take into consideration the latent heat of vaporisation of hydrogen (476 kJ/kg) nor the heat released by the conversion of hydrogen molecules from orthohydrogen to parahydrogen (525 kJ/kg) at temperatures above its boiling point. [40] These effects largely cancel each other out, however as the heat released by the conversion of orthohydrogen to parahydrogen is roughly 10% greater than the latent heat of vaporisation of hydrogen, one can expect the outlet temperature of hydrogen to be slightly greater than shown in calculations.

Fouling is the formation of deposits on heat transfer surfaces and is a common phenomenon in heat exchangers [41]. Common fouling factors are in the order of magnitude of 10^{-3} and would make a negligible difference to the overall heat transfer coefficient in this case, so fouling is ignored in the design of this heat exchanger. Despite this, one may expect ice fouling to occur within this heat exchanger due to the low tube side surface temperature of approximately 130 K and the moisture present in ambient air.

As air temperatures decreases, the ability of air to hold water vapour also decreases. Therefore, this problem is most relevant whilst the aircraft is on the ground or at a low altitude, when the air temperature is highest. One solution for this problem is to use an anti-icing hydrogel [42] on the outer tube side of the heat exchanger. By inhibiting ice nucleation, ice propagation and reducing ice cohesion strength, the hydrogel is able to prevent and delay ice formation. The thermal conductivity of the hydrogel would have to be taken into account when designing the heat exchanger. Other solutions include removing any moisture from the air before it enters the shell side of the heat exchanger. This could be achieved by implementing a bespoke membrane condenser into the design. [43].

In the event that ice was to form within the heat exchanger, the affect on the performance of the heat exchanger can be determined by adding an additional term to equation (40) as shown below

$$U = \left(\frac{1}{h_{air}} + \frac{x_{ice}}{\lambda_{ice}} + \frac{x_{al}}{\lambda_{al}} + \frac{1}{h_{h_2}} \right)^{-1} \quad (40)$$

where x_{ice} is the thickness of the ice layer and λ_{ice} is the thermal conductivity of ice. A 5 mm layer of ice with a thermal conductivity of 4 W/mK [44] would reduce the outlet temperature of the hydrogen to 73.4 K at a hydrogen mass flow rate of 0.588 kg/s and an air mass flow rate of 6 kg/s. This issue can be overcome by driving a higher mass flow rate of air through the shell side of the heat exchanger.

Table 7: Parameters used to determine heat transfer area of heat exchanger [45] [46]

Parameter	Value	Notes
$T_{c,o}$	150 K	Minimum target outlet temperature of cold fluid at cruising
$T_{c,i}$	20 K	Cold fluid inlet temperature
$T_{h,i}$	223 K	Hot fluid inlet temperature (Ambient air at cruising)
m_{H_2}	0.02 kg/s	Mass flow rate of hydrogen through tube-side lines when cruising
m_{air}	10.00 kg/s	Mass flow rate of air (shell side) when cruising
c_{p,H_2}	13.20 kJ/kgK	Specific heat capacity of Hydrogen at 120 K, 86 Bar
$c_{p,air}$	1 kJ/kgK	Specific heat capacity of air at 223 K, 0.24 Bar
$c_{p,air}$	1 kJ/kgK	Specific heat capacity of air at 223 K, 0.24 Bar
D_i	80.0 mm	Inner Tube Diameter
D_o	88.2 m	Outer Tube Diameter
μ_{H_2}	5.29×10^{-6} Pa·s	Dynamic Viscosity of Hydrogen at 120 K, 86 Bar
μ_{air}	1.22×10^{-5} Pa·s	Dynamic viscosity of air at 180 K, 0.24 Bar
λ_{H_2}	0.098 W/mK	Thermal conductivity of Hydrogen at 120K 86 Bar
λ_{air}	0.017 W/mK	Thermal conductivity of air at 180K 0.24 Bar
λ_{al}	170 W/mK	Thermal conductivity of Aluminium 2219
t_{al}	4.42 mm	Thickness of tubeside aluminium (For a maximum internal pressure of 86 bar, FOS = 5)

3.5.4 Leak Detection

A breach in either the outer or inner layer of the tanks or pipes within the system could lead to catastrophic failure. To detect a breach, pressure transducers are embedded within the vacuum layers of these systems. Palladium nanoparticle clusters are used to detect hydrogen outside the tanks or pipes. Palladium nanoparticles adsorb hydrogen extremely easily. This causes a change in resistivity of the palladium due to palladium hydride being present. The adsorption also causes a volume increase. Both mechanisms can then be used to generate a sensor output. These nanoparticles can be produced via the polyol method, using polyol, and a palladium precursor dissolved in ethylene glycol. The chosen palladium precursor is sodium tetrachloropalladate ($Na_2PdCl_4 \cdot 3H_2O$). These nanoparticles are placed on a glass substrate and then connected with silver electrodes. An output reading is then taken from these electrodes.

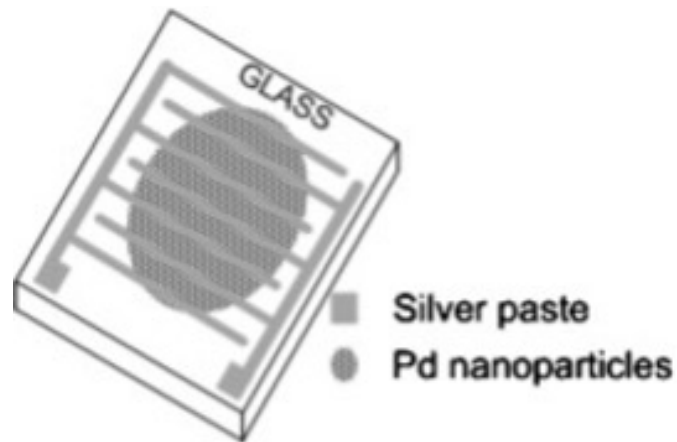


Figure 30: Palladium Hydrogen Sensor [47]

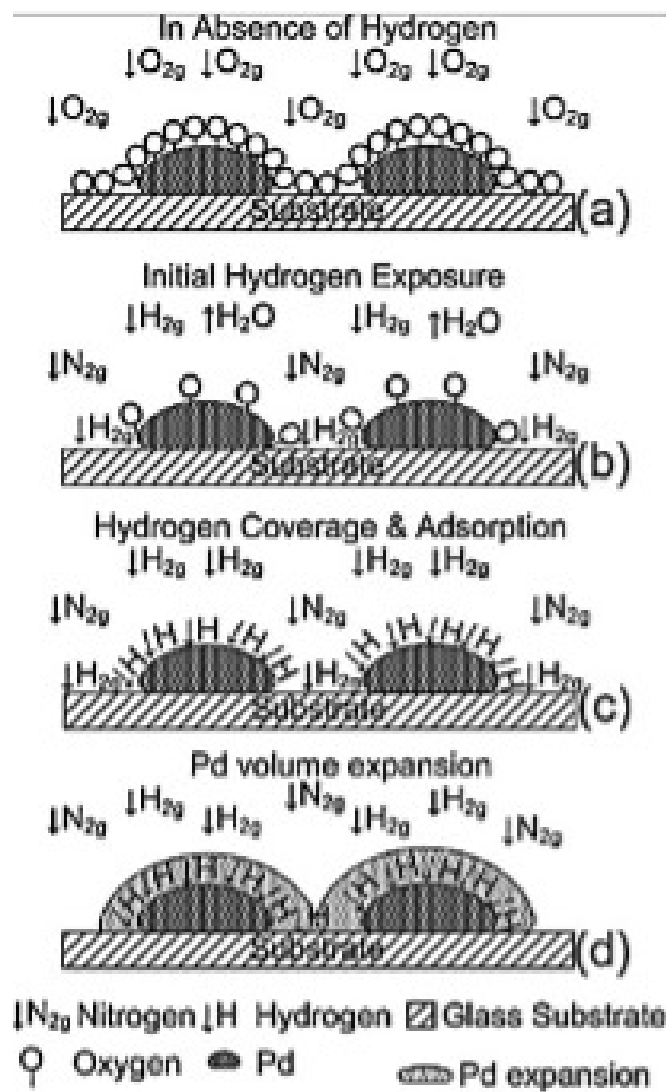


Figure 31: Mechanism of Pd volume expansion [47]

3.5.5 Boost Pump

In order to determine the maximum pump power required, the head loss of the pump was determined from rearrangement of Bernoulli's equation shown (41). Analysis undertaken assumed a constant density of 79 kg/m³, velocity (u) of 13.7 m/s, pressure loss (h_{losses}) from the pipes and the pressure at the pipe exit (outlet) and inlet pump pressure as 86 bar and 1.4 bar respectively. The change in elevation was assumed as negligible in this equation.

$$h_{pump} = \frac{u^2}{2g} + \frac{P}{\rho g_{outlet}} + h_{losses} - \frac{P}{\rho g_{tank}} \quad (41)$$

The pump requirements were calculated using equation (42). The maximum power requirement of the pump was calculated as 94 kW (\dot{W}_{pump}), assuming 100% efficiency, for a maximum pump head loss of 11 km, density of 79 kg/m³ and flow rate of 0.011 m³/s.

$$\dot{W}_{pump} = \frac{\rho g \dot{Q} h_{pump}}{\eta_{pump}} \quad (42)$$

The main design criteria for the pump included high reliability, speed control, high efficiency and a compact design. Options on pump design are outlined in a morphological chart illustrated in Figure 32. A centrifugal pump was determined as the most appropriate because it can operate at variable speeds and is generally used for fluids with a low viscosity such as hydrogen. Due to the location of the pumps, they must be electrically operated since it is inefficient to use the mechanical power of the engine because of extra piping and engineering complexity. Electrically powered pumps have the advantage of more reliable control and the ability to vary the speed using a variable frequency motor. Adaptations are necessary for a pump to operate at 20 K. The pump will require a hermetically sealed design to prevent hydrogen leaks. Using a conventional oil-lubricated steel bearing will not be sufficient due to the potential risk of the oil freezing and alternative options are outlined in Figure 32. Current hybrid-ceramic bearing designs have the most potential because of their low thermal expansion coefficient, approximately $3 \times 10^{-6} \text{ }^\circ\text{C}^{-1}$ [48], compared to 304 stainless steel thermal expansion coefficient of $17 \times 10^{-6} \text{ }^\circ\text{C}^{-1}$ and also removes the need for a lubricant [49].

	Option 1:	Option 2:	Option 3:
Pump type	Centrifugal	Positive Displacement	
Power Source	Hydraulic	Electrical	Engine Bleed Air
Drive Shaft Material	Steel	Carbon Composite	Aluminium
Bearings	Magnetic	Hybrid-ceramic	Steel

Figure 32: Morphological matrix for pump design

The inlet and outlet diameters of the pump were designed as 30 mm for ease of fitting with the liquid phase pipe but can altered if further compressible fluid flow modelling is carried out in the future. The pumps are located at the bottom of the tank to provide more than enough net positive suction head (NPSH) to overcome the vapour pressure of approximately 0.9 bar at 20 K [50]. This is why it was a design requirement to have a pump close to the tank and minimise the risk of cavitation in the pump. This risk can increase if the pump is further away from the tank where the pressure can drop in the piping and fall below the vapour pressure. Two pumps are located on the tank for redundancy and the layout in conjunction with the shutoff valves are shown in Figure 33. A check valve is installed at the outlet of each pump to prevent backwards flow into the pump.

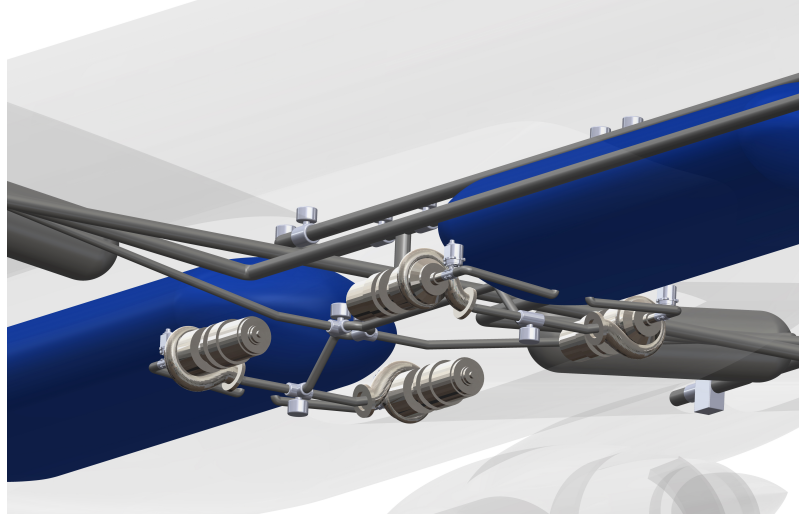


Figure 33: Pump layout arrangement

The pump's output parameters are set by the engine flow demand and tank inlet pressure shown in Figure 34.

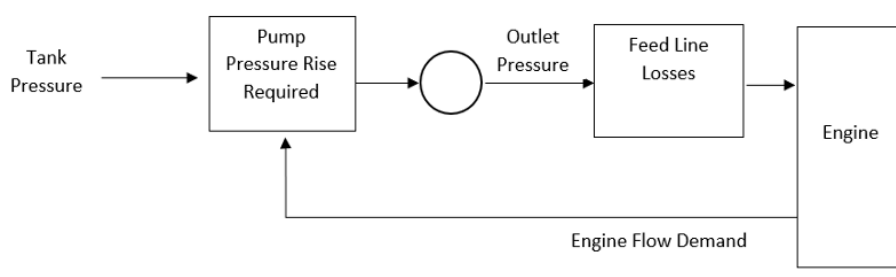


Figure 34: Pump feed system block diagram

3.6 APU Fuel Delivery

The APU found on an aircraft is a small engine that provides electrical power and bleed air for air conditioning onboard whilst the engines are not running and the aircraft is not connected to a ground power unit supply. In conventional systems, although some APUs are certified to operate during flight, the APU is switched off during flight and its role is handled by the engines.

In this fuel system, the APU is intended to be used in-flight to minimise any instances in which hydrogen may need to be vented to the atmosphere, reducing hydrogen losses. The APU is supplied via two pipelines. The first of which connects the flow out of the heat exchanger to the APU and the second of which connects the flow through the VCS and the venting system to the APU. This allows the APU to operate as normal whilst ensuring any hydrogen boil-off can be burned and converted to electricity, providing the aircraft with additional electrical power or to charge an onboard battery. The operating inlet pressure to the APU is often lower than that of the engine. In order to reduce the pressure of the flow supplying the APU from the heat exchanger exit, a pressure regulator can be implemented [51].

4 Sustainability

Primarily tackling UN Sustainable development goals 7 (Affordable and Clean Energy), 9 (Industry, Innovation and Infrastructure) and 13 (Climate Action), this project represents the kind of engineering innovation that is required, moving towards a more sustainable future [52].

Hydrogen is a very promising fuel source as it does not produce CO₂ when burned and can be produced in several different ways such as natural gas reforming, electrolysis and fermentation [53]. As hydrogen can be produced in

several different ways, the environmental impact of producing hydrogen can vary greatly. There are different colours of hydrogen relating to the way in which it is produced, with green hydrogen (produced without emitting CO₂) only representing a small proportion of all hydrogen produced [54]. In 2018, hydrogen production was responsible for around 830 million tonnes of CO₂ emissions [55]. In order to maximise the benefits of using hydrogen as a fuel it needs to be produced using zero carbon, renewable sources of energy.

4.1 NO_x emissions

As mentioned previously, the combustion of hydrogen does not lead to the production of CO₂, however there are still NO_x emissions associated with hydrogen combustion. In a gas engine, combustion takes place in the presence of air and as a consequence, nitrogen is present in the combustion mixture. As a consequence, ‘thermal NO’ is formed. NO then reacts in the atmosphere to form NO₂ which is a harmful air pollutant [56]. This occurs in all instances in which the flame temperature is greater than 1300 °C, which is much lower than hydrogen’s flame temperature of 2127 °C [57].

NO_x emissions could be reduced or eliminated if hydrogen was burned in the absence of nitrogen. Currently, rockets using liquid hydrogen and liquid oxygen as fuel are able to burn hydrogen in the absence of nitrogen. Methods to separate nitrogen from air, such as cryogenic distillation, exist however the most appropriate method for this type of application involves the use of a nitrogen membrane. Unfortunately this technique requires any air passing through the membrane to be clean and dry which brings further challenges given ambient aircraft conditions [58].

4.2 Weight Minimisation

To reduce fuel consumption, it is important to minimise the weight of any systems onboard an aircraft. This is beneficial regarding both sustainable and commercial considerations. Where possible, decisions have been taken to reduce the overall weight of the fuel system without compromising the safety of the system and ensuring sufficient redundancy in crucial elements of the design. The inner carbon tank is an excellent example of this. Using an inner carbon tank over a steel tank results in a 79 % mass reduction.

4.3 Carbon Footprint

In order to estimate the carbon footprint of the design, MakerSite was used. MakerSite uses artificial intelligence to give an idea of the carbon footprint of a product by estimating emissions at several different points along the life of the product including manufacturing and transportation. Table 8 contains the estimated fuel system mass and material composition that was used in MakerSite. According to MakerSite, the manufacturing of the fuel system leads to the emission of 7810 tonnes of CO₂ equivalent. On a popular flight route, London to Berlin, a Boeing 737 emits 11.4 tonnes of CO₂. Considering the CO₂ emissions of a daily flight from London to Berlin, a similar plane using this fuel system would be able to offset its own manufacturing emissions within just 2 years of service. This demonstrates the enormous potential impact of using green hydrogen as a fuel.

Table 8: Estimated fuel system mass and predominant material composition. (*Material with highest percentage composition by mass taken to be the only material of said system component)

System Component	Mass	Material	Composition by Mass /%
Tanks	3100	Steel Carbon Fibre Reinforced Polymer	89 10
Heat Exchanger	150	Aluminium	100*
Pumps	500	Steel	100*
Pipelines	100	Steel	100*
Total Weight	3850		

5 Safety

Safety is of the utmost importance in commercial aviation. Figure 35 lists several hazards associated with the fuel system and ways in which these hazards are mitigated.

Hazard	Risk	Mitigation
Cryogenic Temperatures	<ul style="list-style-type: none"> • Frostbite • Boil-off • Hydrogen embrittlement 	<ul style="list-style-type: none"> • Ensure materials are well insulated • Ensure hardness of stainless steels are low, surface coatings are used and heat-treated during manufacturing.
Source of ignition	<ul style="list-style-type: none"> • Risk of fire is extremely high if hydrogen is within flammability limits. • Minimum ignition energy of 0.02 mJ [59] (10x lower than kerosene) and flammable 	<ul style="list-style-type: none"> • Hydrogen leak detection system • Pressure and temperature sensors to identify hydrogen leaks • Vent exhausting outlets placed on the end of each wing to ensure furthest distance from engines • Computer controlled valves isolate faulty section to stop any further hydrogen leak • Multiple one-way valves prevent the formation of ignitable mixture by ensuring no air can enter the fuel system
Over pressurisation of tank	<ul style="list-style-type: none"> • Tank rupture • At cryogenic temperatures, dense flammable GH2 gas could travel several meters before being dispersed leading to risk of fire. 	<ul style="list-style-type: none"> • Tank ventilation minimises this risk with ventilation system having multiple valves for redundancy, and a cross feed gas GH2 line. • Rupture discs protect tanks from rupturing
Under pressurisation of tank	<ul style="list-style-type: none"> • Air entering tank creates a fire risk • Pump failure 	<ul style="list-style-type: none"> • Implement pressure generation system • Have two pumps on each tank for redundancy • Rupture discs protect tanks from imploding
High internal pressure in pipes	<ul style="list-style-type: none"> • Burst pipe • Hydrogen leak 	<ul style="list-style-type: none"> • Implement factors of safety for max. working stress • Double walled pipes to increase redundancy • Leak detection system
Engine Fire	<ul style="list-style-type: none"> • Engine fire means more fuel may be needed for other engine 	<ul style="list-style-type: none"> • Use LH2 crossfeed • Use control valve to direct flow to the other engine • Shut off valves to prevent more fuel flow to engine on fire
Centre of gravity of plane	<ul style="list-style-type: none"> • Fuel imbalance may move centre of gravity which can cause instability and potentially a crash 	<ul style="list-style-type: none"> • Have a LH2 crossfeed system • Hydrogen is lighter than Kerosene which reduces the change in longitudinal balance of the E190
Lightning	<ul style="list-style-type: none"> • Ignition of fuel within the system 	<ul style="list-style-type: none"> • Venting outlets are placed away from the wingtip • Flame arresters are installed at vent outlets to prevent back flow of flame into the fuel system • Prevent internal sparks by using conductive structural joint in the event of lightning strike [22].

Figure 35: Fuel system hazard mitigation [22], [59]

6 Commercial Considerations

The narrow-body market segment is estimated to account for 67% of new aircraft acquisitions between 2030-50 [60]. This provides a business opportunity to develop a new type of fuel system for an aircraft which allows airlines to meet carbon emission targets and form part of an increasingly used Environmental, Governance and Social (ESG) investment model. Investing in a liquid hydrogen fuel system design for a regional jet is a long-term investment. However, as the cost of manufacturing cryogenic equipment and composite materials declines, the cost of LH₂ powered aircraft will decline. Commercial considerations taken into account when designing the fuel system was passenger and cargo capacity. Placing the tanks underneath the cabin floor ensures the passenger capacity remains the same. Cargo capacity has only been reduced from the original capacity of 22.5 m³ to approximately 19 m³ based on the tank layout design but at the expense of a 53 % reduced fuel range from the original design [61]. However, the fuel range can still cover at least 80 % of flight distances typically used for the Embraer 190 [62]. Material costs have also been considered. The cost of aerospace grade carbon fibre is approximately \$85 / kg compared to cost of aerospace grade aluminium alloy used for aircraft fuel tanks of \$12 / kg [63]. However, the carbon composite market is growing by 15-20 % [62] per year and it is expected advancements in manufacturing techniques will reduce this cost. Other costs include legislation, development of hydrogen safety regulations, and crucially infrastructure to support hydrogen supply chains and production. This is projected to bring the cost of hydrogen down to the same price of kerosene by 2050 [64].

7 Code of Practice

Further to current laws and standards, the following code of practice should be adhered to, in order to ensure the safe operation of the fuel system.

Requirements	Description
Training and expertise	<ul style="list-style-type: none"> Receiving, storing and displacing tasks must be conducted by trained personnel, with annual training undertaken.
Fire risk evaluation	<ul style="list-style-type: none"> Risk when handling fuel, such as flushing air procedures, leaks and vapour emissions Removal of equipment that may induce a source of ignition from the fuelling zone. Fuelling procedures must be in place e.g. bonding connections made before filler caps removed, ensuring electrical discontinuity.
Fuel contamination procedures	<ul style="list-style-type: none"> Regular cleaning procedures in place to prevent fuel contamination in the pipelines and tanks. Also, licensees must have quality control and maintenance procedures in place.
Leak risk evaluation	<ul style="list-style-type: none"> Due to the extremely low viscosity of hydrogen, it is very difficult to prevent the system from leaking. Frequent maintenance must be undertaken and hydrogen leak detection systems must be in place throughout the system.
Clear exit paths for passengers	<ul style="list-style-type: none"> Passengers should disembark prior to the refuelling process. However, where this is impractical the re-fuelling equipment and vehicles must not impede the passengers exit. Therefore, the fuelling pipe should enter under belly on the opposite side to the main passenger door and emergency exit slides.
Emergency stop control	<ul style="list-style-type: none"> A "STOP" button close to each fuelling point to stop the fuel flow immediately.
Fuel quality checks	<ul style="list-style-type: none"> Quality checks should be done periodically on fuel samples taken from the drain cocks of each tank. Until satisfactory checks have been completed, any fuel removed should not be mixed with any uncontaminated fuel. This fuel should be checked for water and sediment. These fuel quality checks should be undertaken before and after fuelling/defueling, after vehicle cleaning and after prolonged heavy rainfall or snow
Portable Electronic Devices (PEDs) risk evaluation	<p>Licensees should be aware of the three primary risks associated with the use of PEDs in the vicinity of aircraft fuel systems.</p> <ul style="list-style-type: none"> PEDs creating or inducing a spark of sufficient intensity can possibly ignite fuel. PED users may be distracted when on site resulting in incomplete safety tasks or damage to the aircraft/user. PEDs have been reported to interfere with fuel gauges within aircraft fuel systems. Such interference could result in an overweight take-off due to excessive fuel or a flight with insufficient fuel
Record Keeping	<ul style="list-style-type: none"> Written records should be kept of fuel quality tests, equipment checks, pressure checks etc.

Figure 36: Code of Practice

8 Discussion

The fuel system design meets the user requirement specification outlined in the project scope in order to achieve the project goal of designing a LH₂ fuel system for the Embraer 190. For example, functional redundancies are included at every stage of the fuel system such as two boost pumps for each tank and four ways to ventilate the tank. Complying with industry standards for factors of safety means that pipes and tanks can reliably operate under high internal pressures. The total mass of the fuel system designed was estimated at 3850 kg shown in Table 8. The mass of the fuel system including the fuel was added to the basic operating mass, 27,753 kg, of the original E190. Therefore, the maximum mass of the aircraft without payload is 33,017 kg. This falls below the maximum landing mass of 43,000 kg, meeting the target requirements. This causes a 13 % maximum payload mass reduction from the original E190. However, this is a conservative estimation because the basic operating mass of the original E190 included the existing fuel system.

In conventional aircraft fuel systems, fuel is stored in the wings of the aircraft. Fuel stored in the wings acts against the direction of stress induced in the wings throughout the duration of the flight, particularly shortly after takeoff [65]. The weight of the fuel also helps to reduce a phenomenon known as wing flutter. Wing flutter describes unstable vibrations of the wing that occur due to the flow of air around the wing, which can cause catastrophic failure [66]. Due to the volume and shape requirements of the LH₂ tanks, it is not feasible to store LH₂ in the wings of the aircraft. As a consequence, the wings of the aircraft may need to be reinforced to withstand higher bending moments and to reduce wing flutter.

Before commercial hydrogen powered aircraft take to the skies, the supporting hydrogen infrastructure must be developed. As discussed in [67], airports catering for hydrogen powered aircraft would ideally have hydrogen production and storage facilities onsite in order to minimise hydrogen losses that may occur whilst transporting the hydrogen from a production facility to an airport apron. Widespread availability of hydrogen at airports and a lack of supporting infrastructure could well be the limiting factor in the adoption of hydrogen as a primary aviation fuel.

The aviation giant Airbus has also recognised hydrogen as the fuel of the future having announced its ZEROe project and plans to release the first zero emissions commercial aircraft by 2035. Recently, they announced the launch of their ZEROe demonstrator programme in which they are planning to test hydrogen technologies in flight. Most notably with a hydrogen gas engine attached to an A380 test bed [68]. These types of programmes, that aim to demonstrate and test hydrogen technologies, will prove to be vital in order to improve the public perception of the safety of hydrogen as a fuel for commercial aviation. In a survey conducted in 2019 by the World Economic Forum, only 49.5 % of respondents believed hydrogen is generally safe [69]. Extensive testing will be necessary to prove the safety of hydrogen systems and remove current hydrogen technologies from disasters such as the Hindenburg airship disaster of 1937 [70].

9 Further Work

The wider goal of this project was to tackle the climate emergency, and for this hydrogen fuel system to be developed for commercial use. Before this can be achieved, further work and testing needs to be carried out on the proposed system.

Areas of further work include conducting bending tests and a failure analysis in a laboratory to support the theoretical analysis presented in section 3.4, in order to obtain experimental verification that the tank can withstand external loads and the internal pressure. In addition, further material research focused on composites for cryogenic applications could have an enormous impact on the design. As quoted in Table 8, steel contributes to 89 % of the overall tank weight. Further research supported by experimental data could determine whether carbon fibre reinforced polymers could replace steel in the system. This could significantly reduce the weight of the aircraft, saving fuel, or increasing the range of the aircraft. The reduction or elimination of NO_x emissions could be tackled by developing an appropriate method of separating hydrogen from air to ensure it is not present in the combustion chamber of the engine, or by developing a system that also stores liquid oxygen and burns hydrogen with pure oxygen.

10 Conclusion

This report discusses the design of a hydrogen fuel system for gas engines, in which hydrogen is stored as LH₂ in two tanks under the cabin floor of the Embraer 190. With a total tank volume of 20.53m³ and LH₂ weight of 1414 kg, the range of the Embraer 190 is approximately 2000 km, which is large enough to serve the top 20 busiest flight routes in Europe [71]. The tank venting system described in the report ensures the pressure within the tank stays within an operating range of 1.35 ± 0.05 bar, and includes rupture disks to prevent excessive pressure building up within the tank. Before delivery to the engines, the LH₂ is gasified in heat exchangers located in each wing of the aircraft. A major concern when storing cryogenic liquids is boil-off. The fuel system described takes advantage of boil-off to further reduce any heat leak into tank, via the VCS, before delivering boil-off to the APU where it can be burned and converted into electrical energy. The fuel system described demonstrates the viability of hydrogen powered commercial aviation and zero emission air travel. Given the climate emergency, the implementation of this fuel system and the development of green hydrogen technologies is both pertinent and necessary to ensure industries and governments across the world move towards net zero carbon emissions.

11 Project Schedule

Shown in Figure 37 Gantt chart detailing key tasks split into manageable time frames and the total staff cost fell under the budget of £14,400. Some deadlines were extended from what was originally planned but key milestones such as publishing the final report were successfully completed on time.

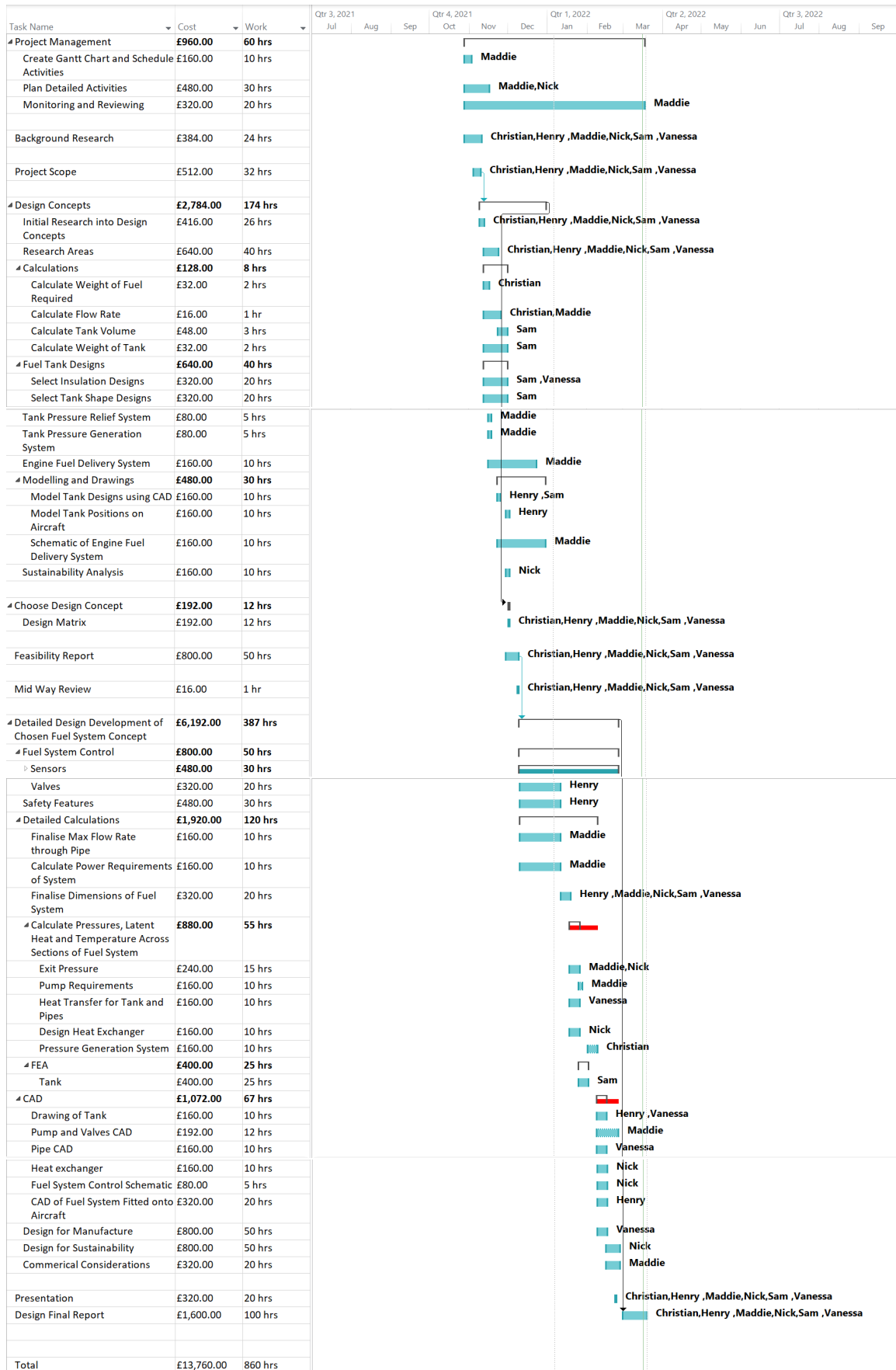


Figure 37: Gantt Chart

References

- [1] Deloitte, “Decarbonizing aerospace.” <https://www2.deloitte.com/uk/en/insights/industry/aerospace-defense/decarbonizing-aerospace.html>.
- [2] Air Transport Action Group, “Facts and figures.” <https://www.atag.org/facts-figures.html>. [Online] Accessed 15-03-2022.
- [3] Department for Business, Energy and Industrial Strategy, “Uk hydrogen strategy.” https://assets.publishing.service.gov.uk/government/uploads/system/uploads/attachment_data/file/1011283/UK-Hydrogen-Strategy_web.pdf. [Online] Accessed 15-03-2022.
- [4] K. T. Møller, T. R. Jensen, E. Akiba, and H. wen Li, “Hydrogen - a sustainable energy carrier,” *Progress in Natural Science: Materials International*, vol. 27, no. 1, pp. 34–40, 2017. SI-HYDROGEN STORAGE MATERIALS.
- [5] US Energy Information Administration, “Hydrogen explained.” <https://www.eia.gov/energyexplained/hydrogen/use-of-hydrogen.php>. [Online] Accessed 15-03-2022.
- [6] “Hydrogen-powered aviation a fact-based study of hydrogen technology, economics, and climate impact by 2050.” McKinsey Company, Clean Sky 2 and FCH 2 JU, p.26, p48.
- [7] S. B. Rayhan, X. Pu, and X. Huilong, “Modeling of fuel in crashworthiness study of aircraft with auxiliary fuel tank,” *International Journal of Impact Engineering*, vol. 161, p. 104076, 2022.
- [8] International Civial Aviation Organization, “Icao annex 6, 4.3.6 fuel requirements.” <https://www.pilot18.com/wp-content/uploads/2017/10/Pilot18.com-ICAO-Annex-6-Part-1-Operation-of-Aircraft-International-aeroplane.pdf>. [Online] Accessed 13-03-2022.
- [9] D. Plachta and P. Kittel, “An update to zero boil-off cryogenic propellant storage analysis applied to upper stages or depots in a leo environment,” in *38th AIAA/ASME/SAE/ASEE joint propulsion conference & exhibit*, p. 3589, 2002.
- [10] C. Winnefeld, T. Kadyk, B. Bensmann, U. Krewer, and R. Hanke-Rauschenbach, “Modelling and designing cryogenic hydrogen tanks for future aircraft applications,” *Energies*, vol. 11, no. 1, p. 105, 2018.
- [11] American Society of Mechanical Engineers, *Boiler and Pressure Vessel Code*, vol. 1. 2017.
- [12] S. L. Schnulo, D. L. Hall, J. C. Chin, and A. D. Smith, “Further development of the nasa x-57 maxwell mission planning tool for mods ii, iii, and iv,” in *2019 AIAA/IEEE Electric Aircraft Technologies Symposium (EATS)*, pp. 1–14, IEEE, 2019.
- [13] G. Letchworth, “X-33 reusable launch vehicle demonstrator, spaceport and range,” in *AIAA Space 2011 Conference & Exposition*, p. 7314, 2011.
- [14] A. Petras, *Design of sandwich structures*. PhD thesis, University of Cambridge, 1999.
- [15] J. de Dios Rodriguez, *Analysis of the nonlinear behavior of inserts in sandwich structures: application to an innovative sizing method*. PhD thesis, INSA de Toulouse, 2018.
- [16] A. G. L. C. Keller, G. Cunningham, “Thermal performance of multilayer insulations nasa contractor report cr-134477.” <https://ntrs.nasa.gov/api/citations/19740014451/downloads/19740014451.pdf>, 1974. [Online] Accessed 13-03-2022.
- [17] E. Ramírez-Laboreo, C. Sagüés, and S. Llorente, “Thermal modeling, analysis and control using an electrical analogy,” in *22nd Mediterranean Conference on Control and Automation*, pp. 505–510, IEEE, 2014.
- [18] R. B. Scott, “Thermal design of large storage vessels for,” *Journal of Research of the National Bureau of Standards*, vol. 58, no. 6, p. 317, 1957.
- [19] S. Kulsa, “How to make cryogenic multi-layer insulation (mli) shields.” <https://hydrogen.wsu.edu/2020/06/16/how-to-make-cryogenic-multi-layers-insulation-mli-shields/>, 2020. [Online] Accessed 10-03-2022.
- [20] Z. Liu, Y. Li, F. Xie, and K. Zhou, “Thermal performance of foam/mli for cryogenic liquid hydrogen tank during the ascent and on orbit period,” *Applied Thermal Engineering*, vol. 98, pp. 430–439, 2016.
- [21] J. J. Darji, “Heat transfer through a honeycomb sandwich panel,” 1963.
- [22] N. R. Council *et al.*, *Aviation fuels with improved fire safety: a proceedings*. National Academies Press, 1997.
- [23] R. Langton, C. Clark, M. Hewitt, and L. Richards, *Aircraft fuel systems*. John Wiley & Sons, 2009.
- [24] J. J. Zipay, C. T. Modlin, and C. E. Larsen, “The ultimate factor of safety for aircraft and spacecraft-its history, applications and misconceptions,” in *57th AIAA/ASCE/AHS/ASC Structures, Structural Dynamics, and Materials Conference*, p. 1715, 2016.
- [25] GE Aviation, “Datasheet cf43-10e.” <https://www.geaviation.com/sites/default/files/datasheet-CF34-10E.pdf>. [Online] Accessed 10-03-2022.
- [26] EASA, “Type cf34-10e series engines.” <https://www.easa.europa.eu/sites/default/files/dfu/CF34->

- 10EseriesTCDSissue6.pdf, 2020. [Online] Accessed 1-03-2022.
- [27] Engineering Toolbox, “Roughness and surface coefficients.” https://www.engineeringtoolbox.com/surface-roughness-ventilation-ducts-d_209.html. [Online] Accessed 1-03-2022.
- [28] Neutrium, “Pressure loss from fittings.” <https://neutrium.net/fluid-flow/pressure-loss-from-fittings-excess-head-k-method/>. [Online] Accessed 1-03-2022.
- [29] M. Toghraei, “Origin of “erosional velocity formula”.” <http://engedu.ca/wp-content/uploads/Origin-of-Maximum-Velocity-formulae-Rev.-11.pdf>, 2013. [Online] Accessed 1-03-2022.
- [30] PAM Saint Gobain, “Safety factor.” <https://www.pamline.com/catalog/our-products/other-links/technical-information/project-design/pressure-and-angular-deviation-joint/safety-factor>. [Online] Accessed 1-03-2022.
- [31] J. A. Demko, J. Fesmire, and S. Augustynowicz, “Design tool for cryogenic thermal insulation systems,” in *AIP Conference Proceedings*, vol. 985, pp. 145–151, American Institute of Physics, 2008.
- [32] W. L. Armarego, *Purification of laboratory chemicals*. Butterworth-Heinemann, 2017.
- [33] Total Materia, “Properties of aluminum alloys at cryogenic and elevated temperatures.” <https://www.totalmateria.com/Article23.htm>. [Online] Accessed 10-03-2022.
- [34] A. Gomez and H. Smith, “Liquid hydrogen fuel tanks for commercial aviation: Structural sizing and stress analysis,” *Aerospace Science and Technology*, vol. 95, p. 105438, 2019.
- [35] T. L. Bergman, F. P. Incropera, D. P. DeWitt, and A. S. Lavine, *Fundamentals of heat and mass transfer*. John Wiley & Sons, 2011.
- [36] M. Nitsche and R. O. Gbadamosi, *Heat exchanger design guide: a practical guide for planning, selecting and designing of shell and tube exchangers*. Butterworth-Heinemann, 2015.
- [37] Engineering ToolBox (2005), “International standard atmosphere.” https://www.engineeringtoolbox.com/international-standard-atmosphere-d_985.html. [Online] Accessed 10-03-2022.
- [38] A. S. Jursa *et al.*, *Handbook of geophysics and the space environment*, vol. 1. Air Force Geophysics Laboratory, Air Force Systems Command, United States . . . , 1985.
- [39] Skybrary, “Embraer erj 190-100.” <https://skybrary.aero/aircraft/e190>. [Online] Accessed 13-03-2022.
- [40] R. M. Bliesner, *Parahydrogen-orthoohydrogen conversion for boil-off reduction from space stage fuel systems*. PhD thesis, Washington State University Pullman, 2013.
- [41] H. Müller-Steinhagen, M. Malayeri, and A. Watkinson, “Heat exchanger fouling: mitigation and cleaning strategies,” 2011.
- [42] Z. He, C. Wu, M. Hua, S. Wu, D. Wu, X. Zhu, J. Wang, and X. He, “Bioinspired multifunctional anti-icing hydrogel,” *Matter*, vol. 2, no. 3, pp. 723–734, 2020.
- [43] A. Brunetti, F. Macedonio, G. Barbieri, and E. Drioli, “Membrane condenser as emerging technology for water recovery and gas pre-treatment: Current status and perspectives,” *BMC Chemical Engineering*, vol. 1, no. 1, pp. 1–15, 2019.
- [44] Engineering Toolbox, “Ice - thermal properties.” https://www.engineeringtoolbox.com/ice-thermal-properties-d_576.html. [Online] Accessed 13-03-2022.
- [45] Aubert Duval, “Aluminium alloy 2219 datasheet.” https://www.aubertduval.com/wp-media/uploads/sites/2/pdf/2219_GB.pdf. [Online] Accessed 10-03-2022.
- [46] Wolfram Research Inc., “Wolfram alpha science and technology.” <https://www.wolframalpha.com>.
- [47] D. Gupta, D. Dutta, M. Kumar, P. Barman, C. Sarkar, S. Basu, and S. Hazra, “A low temperature hydrogen sensor based on palladium nanoparticles,” *Sensors and Actuators B: Chemical*, vol. 196, pp. 215–222, 2014.
- [48] C.-L. Tien and T.-W. Lin, “Thermal expansion coefficient and thermomechanical properties of sin x thin films prepared by plasma-enhanced chemical vapor deposition,” *Applied optics*, vol. 51, no. 30, pp. 7229–7235, 2012.
- [49] W. D. Callister and D. G. Rethwisch, *Materials science and engineering: an introduction*, vol. 9. Wiley New York, 2018.
- [50] R. B. Scott, W. H. Denton, and C. M. Nicholls, *Technology and uses of liquid hydrogen*. Elsevier, 2013. Table 2A, Chapter 11, p381.
- [51] IMI Norgen, “J50 spring loaded regulator datasheet.” http://cdn.norgren.com/pdf/en_8_810_150_J50.pdf. [Online] Accessed 15-03-2022.
- [52] U. Nations.
- [53] US Department of Energy, “Hydrogen production and distribution.” https://afdc.energy.gov/fuels/hydrogen_production.html. [Online] Accessed 13-03-2022.
- [54] National Grid, “The hydrogen colour spectrum.” <https://www.nationalgrid.com/stories/energy-explained/hydrogen-colour-spectrum>. [Online] Accessed 13-03-2022.
- [55] IEA, “The future of hydrogen.” <https://www.iea.org/reports/the-future-of-hydrogen>, 2019. [Online]

Accessed 13-03-2022.

- [56] A. C. Lewis, "Optimising air quality co-benefits in a hydrogen economy: a case for hydrogen-specific standards for no x emissions," *Environmental Science: Atmospheres*, vol. 1, no. 5, pp. 201–207, 2021.
- [57] I. Glassman, R. A. Yetter, and N. G. Glumac, "Chapter 1 - chemical thermodynamics and flame temperatures," in *Combustion (Fifth Edition)* (I. Glassman, R. A. Yetter, and N. G. Glumac, eds.), pp. 1–40, Boston: Academic Press, fifth edition ed., 2015.
- [58] Atlas Copco, "Generating nitrogen using membrane technology." <https://www.atlascopco.com/en-uk/compressors/wiki/compressed-air-articles/generating-nitrogen-membrane>. [Online] Accessed 13-03-2022.
- [59] Flyzero, "Hydrogen infrastructure and operations," 2022. p. 9.
- [60] Aerospace Technology Institute, "Flyzero – zero-carbon emission aircraft concepts report," 2022.
- [61] Embraer, "Embraer 190 airport planning manual," 2021. p 2-2.
- [62] P. J. Simple Flying, "The world's longest embraer e190/195 routes." <https://simpleflying.com/the-worlds-longest-embraer-e190-195-routes/>, 2021. [Online] Accessed 9-03-2022.
- [63] Infosys, "Carbon composites are becoming competitive and cost effective." <https://www.infosys.com/engineering-services/white-papers/documents/carbon-composites-cost-effective.pdf>, 2018. [Online] Accessed 13-03-2022.
- [64] McKinsey Company, 2020, "Hydrogen-powered aviation a fact-based study of hydrogen technology, economics, and climate impact by 2050." https://www.fch.europa.eu/sites/default/files/FCH%20Docs/20200507-Hydrogen%20Powered%20Aviation%20report_FINAL%20web%20%28ID%208706035%29.pdf, 2018. Clean Sky 2 and FCH 2 JU, p.48. [Online] Accessed 13-03-2022.
- [65] AN Aviation Services, "Why is fuel stored in the wings of aircraft?." <https://an.aero/why-is-fuel-stored-in-the-wings-of-aircraft/>.
- [66] C. Bibin, M. J. Selvaraj, and S. Sanju, "Flutter analysing over an aircraft wing during cruise speed," *Procedia Engineering*, vol. 38, pp. 1950–1961, 2012. INTERNATIONAL CONFERENCE ON MODELLING OPTIMIZATION AND COMPUTING.
- [67] Airbus, "Tomorrow's airports: future energy ecosystems?." <https://www.airbus.com/en/newsroom/news/2021-06-tomorrows-airports-future-energy-ecosystems-0>.
- [68] Airbus, "The zeroe demonstrator has arrived." <https://www.airbus.com/en/newsroom/stories/2022-02-the-zeroe-demonstrator-has-arrived>.
- [69] World Economic Forum, "Hydrogen power is safe and here to stay." <https://www.weforum.org/agenda/2019/04/why-don-t-the-public-see-hydrogen-as-a-safe-energy-source/>.
- [70] G. D. Brewer, *Hydrogen aircraft technology*. Routledge, 2017.
- [71] Eurostat, "Air transport." <https://ec.europa.eu/eurostat/web/transport/data/database>.

Contributions

Table 9: Project Contributors

Section	Lead Authors	Reviewed
1. Introduction	Christian Garry	Maddie Hall
2. Project Scope	Maddie Hall	Nicholas Njopa-Kaba
3.1 Overall Fuel System Architecture	Nicholas Njopa-Kaba	Samuel Berry
3.2 Weight Requirements	Maddie Hall	Henry Wong
3.3 Range Estimation	Samuel Berry	Vanessa Ohanebo
3.4.1 Tank Placement	Henry Wong	Nicholas Njopa-Kaba
3.4.2 Tank Sizing and Dimensions	Samuel Berry	Maddie Hall
3.4.3 Tank Materials	Vanessa Ohanebo	Henry Wong
3.4.4 Tank Insulation Methods	Vanessa Ohanebo	Christian Garry
3.4.5 LH2 Crossfeed System	Maddie Hall	Nicholas Njopa-Kaba
3.4.6 Tank Venting System	Henry Wong	Samuel Berry
3.4.7 Pressure Generation System	Christian Garry	Vanessa Ohanebo
3.4.8 Tank Level Sensing	Christian Garry	Maddie Hall
3.4.9 Tank Temperature and Pressure	Christian Garry	Henry Wong
3.4.10 Fuelling and Defuelling	Samuel Berry	Nicholas Njopa-Kaba
3.4.11 Tank Cut-outs and Stress Analysis	Samuel Berry	Christian Garry
3.5.1 Line Sizing	Maddie Hall	Christian Garry
3.5.2 Pipe Insulation	Vanessa Ohanebo	Henry Wong
3.5.3 Heat Exchanger	Nicholas Njopa-Kaba	Samuel Berry
3.5.4 Leak Detection	Christian Garry	Maddie Hall
3.5.5 Boost Pump	Maddie Hall	Nicholas Njopa-Kaba
3.6 APU Fuel Delivery	Nicholas Njopa-Kaba	Vanessa Ohanebo
4. Sustainability	Nicholas Njopa-Kaba	Henry Wong
5. Safety	Henry Wong	Maddie Hall
6. Commercial Considerations	Maddie Hall	Samuel Berry
7. Code of Practice	Samuel Berry	Vanessa Ohanebo
8. Discussion	Christian Garry	Nicholas Njopa-Kaba
9. Further Work	Vanessa Ohanebo	Henry Wong
10. Conclusion	Henry Wong	Nicholas Njopa-Kaba

Project Manager: Nicholas Njopa-Kaba

Project Planner: Maddie Hall